REPORT
doi:10.26443/seismica.v5i1.2044

Lower St. Lawrence Seaway Amphibious Seismic Network for earthquakes and marine soundscape monitoring

Yajing Liu [*1], **Alexandre Plourde** [2,3], **Graeme Cairns** [3], **Katie Bosman** [3], **John Thibodeau** [3], **Elahe Sirati** [3], **Justin Chien** [1], **Fiona A. Darbyshire** [4], **Mladen Nedimović** [3], **Miao Zhang** [3], **Wenqiang Zhang** [1,5], **Jian Xu** [1], **Pinar Gurun** [3], **Forde Nedimović** [3]

[1]Department of Earth and Planetary Sciences, McGill University, Montréal, Canada, [2]Natural Resources Canada, Geological Survey of Canada Atlantic, Dartmouth, Canada, [3]Department of Earth and Environmental Sciences, Dalhousie University, Halifax, Canada, [4]Centre de recherche Geotop/Département des sciences de la Terre et de l'atmosphère, Université du Québec à Montréal, Montréal, Canada, [5]Now at Department of Geophysics, Stanford University, Stanford, United States

Author contributions: *Conceptualization*: Y. Liu, A. Plourde, F. A. Darbyshire, M. Nedimović, M. Zhang. *Field operation*: G. Cairns, K. Bosman, J. Thibodeau, M. Nedmović, P. Gurun, F. Nedimović, A. Plourde, J. Chien, E. Sirati, Y. Liu, F. A. Darbyshire, W. Zhang, J. Xu. *Formal Analysis*: Y. Liu, A. Plourde, J. Chien, E. Sirati. *Writing - Original draft*: Y. Liu, A. Plourde. *Writing - Review & Editing*: F. A. Darbyshire, G. Cairns, K. Bosman, J. Chien, M. Nedimović, M. Zhang, J. Xu. *Visualization*: Y. Liu, A. Plourde, J. Chien. *Data curation*: K. Bosman, J. Chien. *Funding acquisition*: Y. Liu, A. Plourde, F. A. Darbyshire, M. Nedimović, M. Zhang.

Abstract The Lower St. Lawrence Seaway (LSLS) is located within one of the most active seismic zones in eastern Canada. It is also home to a range of marine mammals in an environment of intensive fishing and cargo shipping. With the dual objectives to better understand the geohazards and marine soundscape, we operated along the LSLS an amphibious seismic network consisting of 8 broadband ocean bottom seismometers (OBS), 48 short-period nodal sensors, and 4 broadband land stations, with various operation periods between 2023 and 2025. This report documents the deployments, examines data quality, and presents preliminary results from the first month of OBS recording. The OBS recordings show higher noise levels across all frequencies compared to the land broadband stations, with particularly high noise between periods of 0.2–2 s and >10 s on the horizontal components. Long-period noise amplitude correlates closely with tidal cycles, suggesting tidally modulated riverbed currents are the primary cause. The seismicity catalog from combined OBS and land stations shows two times more earthquakes than the Canadian National Earthquake Database in the first month of deployment, as well as many suspected blasts. We also show clear detections of fin whale and blue whale calls at multiple OBS sites, illustrating the potential for whale call location.

Résumé La voie maritime du Bas-Saint-Laurent (BSL) se situe dans l'une des zones les plus exposées aux séismes de l'est du Canada. Elle abrite également une faune marine diversifiée, dans un contexte de pêche intensive et de transport maritime de marchandises. Afin de mieux comprendre les risques sismiques et le paysage sonore marin, nous avons déployé un réseau amphibie de capteurs comprenant huit sismomètres océanique (OBS) dans la BSL, ainsi que 48 sismomètres nodaux et quatre sismomètres à large bande le long du littoral, selon différentes périodes d'exploitation entre 2023 et 2025. Ce rapport documente les déploiements, examine la qualité des données et présente les résultats préliminaires du premier mois d'enregistrement OBS. Les enregistrements des OBS présentent des niveaux de bruit plus élevés que ceux des stations terrestres, avec un bruit particulièrement élevé pour les périodes comprises entre 0,2 et 2 s et supérieures à 10 s sur les composantes horizontales. L'amplitude du bruit aux longues périodes est fortement corrélée aux cycles de marée, ce qui suggère que les courants de fond de rivière modulés par les marées en sont la cause principale. Le catalogue sismique des OBS a deux fois plus d'événements que la Base de données nationale sur les séismes du Canada au cours du premier mois de déploiement, ainsi que de nombreuses explosions présumées. Nous montrons également des détections claires de vocalisations de rorquals communs et de baleines bleues sur plusieurs sites d'observation, illustrant le potentiel de suivi des baleines individuelles.

Production Editor:
Gareth Funning
Handling Editor:
Lise Retailleau
Copy & Layout Editor:
Hannah F. Mark

Signed reviewer(s):
Zoe Krauss
Laura Parisi

Received:
October 10, 2025
Accepted:
May 1, 2026
Published:
May 21, 2026

1 Introduction

The St. Lawrence paleorift system between the Grenvillian basement and the Appalachian nappes in eastern North America has a rich geological heritage punctuated by tectonic events over the past billion years. The Charlevoix Seismic Zone and Lower St. Lawrence Seismic Zone are both located along the paleorift system and have hosted five earthquakes of magnitude 6 and greater since the 17th century, with the most recent (magnitude 6.2) in 1925. The average seismicity rates for these two regions are ~200 and 60 earthquakes per year reported by the Canadian National Earthquake Database (NEDB) catalog (NRCan, 1985), respectively, ranking them the highest seismic hazard regions in

*Corresponding author: yajing.liu@mcgill.ca

eastern Canada (Lamontagne et al., 2003). The majority of earthquakes are located beneath the St. Lawrence River, potentially posing further submarine landslide and tsunami risks to offshore infrastructure and coastal communities. Sedimentological records also revealed that historic and prehistoric earthquakes triggered turbidity currents and the deposition of turbidites in the St. Lawrence Estuary and Saguenay Fjord during the Holocene (Mérindol et al., 2022; St-Onge et al., 2012). In the Lower St. Lawrence Seismic Zone, a system of normal faults with km-scale throw crosscuts both the Precambrian basement and the overlying Ordovician sedimentary layer. These local faults are hypothesized to be weak because of crustal fluids at depth or fault gouges that exhibit a low friction coefficient (Lamontagne et al., 2003). A recent earthquake relocation study by Plourde and Nedimović (2021) suggests seismically-active lineations up to ∼40 km long may be capable of generating magnitude 6 or larger earthquakes. However, due to the sparse Canadian National Seismographic Network (CNSN) station coverage (inter-station distancing on average 100 km), the uncertainties of event locations are too high to identify seismicity clusters and pinpoint correlation to active faults. The lack of station coverage thus directly results in the lack of a detailed understanding of earthquake sources, crustal stress state, and potential triggering of submarine landslides; and consequently high uncertainties in geohazard models.

The Lower St. Lawrence Seaway (LSLS), a term we use to encompass the Estuary and northwestern Gulf of St. Lawrence, has bathymetric and ocean circulation characteristics that create regions of high biological productivity and critical foraging areas for many marine species, including endangered baleen whales. The LSLS is also critical to Canada's economy as part of a major marine shipping corridor and a site of intensive fishing. This cohabitation can create conflict, as baleen whales can be killed from collision with vessels and entanglement with fishing gear, and anthropogenic noise can interfere with their acoustic communication. As such, close monitoring of the LSLS marine soundscape will provide critical information for conservation policies, including monitoring of the whale populations, quantification of marine traffic noise and description of the variability of the natural contributors (e.g., marine mammals, meteorological events). Hydrophone deployments in the LSLS have shown evidence of widespread presence of blue whales and fin whales (Simard et al., 2016a; Roy et al., 2018) and allowed detailed description of the noise level radiated by commercial traffic (Simard et al., 2016b). However, the sparse coverage of hydrophones, with 100+ km interstation distances, often hinders the extent and variability of these marine soundscape observations. More recently Plourde and Nedimović (2022) and Goblot et al. (2024) detected fin and blue whale calls transmitted from the water to the sediment/bedrock and recorded by land seismometers along the shorelines. The continuous land seismic station recording provides year-long whale call catalogs, but the detection radius is limited to a few kilometers, likely due to energy loss in transmission, much less than the typical range of ∼100 km by hydrophones in the Estuary and Gulf of St. Lawrence (Simard et al., 2016a; Roy et al., 2018).

Ocean bottom seismometer (OBS) experiments have proven to be a versatile tool not only for detecting and characterizing earthquakes where land-based networks have limited detection capability, but also for passively recording a broad spectrum of ambient signals that reflect the dynamic marine environment. Previous studies using OBS networks have captured local and regional earthquake sequences, providing critical constraints on fault geometry, crustal structure, and seismogenic zone behavior in offshore settings (e.g., McGuire et al., 2012; Savage et al., 2017; Kuna et al., 2019; Gong and Fan, 2022). Beyond seismicity, OBS records are increasingly recognized as rich archives of environmental and biological noise, including oceanic microseisms, ocean currents, sea ice, marine traffic, and the vocalization of marine mammals (e.g., Wilcock, 2012; Corela et al., 2023; Parisi et al., 2024; Schlindwein et al., 2025).

The LSLS Amphibious Seismic Network (LSLS-ASN) is designed to overcome the aforementioned spatial and/or temporal observational limitations to serve the dual purpose of continuously monitoring seismicity and the marine soundscape of the Lower St. Lawrence region. The LSLS-ASN consists of a network of 8 broadband OBSs, 4 broadband land stations, and 48 short-period nodal sensors with variable deployment periods in 2023-2025, in addition to 5 CNSN permanent broadband stations (Figure 1). While microseism signals generated by ocean waves and solid Earth interaction are well documented phenomena in seismic data, other noise types such as from sensor-seafloor coupling and interference from movements of OBS instrument parts have also been documented and need to be corrected (e.g., Janiszewski et al., 2019; Essing et al., 2021). The unique LSLS physical oceanographic conditions in an estuary that serves as a busy shipping corridor may present further challenges compared to OBS data recorded in the open oceans. Comprehensive documentation of data quality and noise characteristics is required prior to applying the dataset in earthquake and environmental studies. In this report, we document the LSLS-ASN experiment and present data quality assessment, including power spectral density quantification, illustration of example signals and discussion of possible sound sources. We also present preliminary seismicity catalogs and whale call detections derived from recordings in the first month of the experiment. Based on the preliminary results, we also discuss prospects of future projects that could be enabled by the LSLS-ASN dataset.

2 The LSLS Amphibious Seismic Network

The LSLS-ASN consisted of 8 broadband OBSs, 4 broadband land stations, and 48 short-period nodal sensors deployed in 2023-2025, covering the Lower St. Lawrence seismic zone from Les Escoumins to Sept-Îles (Figure 1). The eight OBSs were deployed from September 2023 to May 2024 in Year 1 of the experiment, and from November 2024 to April 2025 in Year 2. Their operation periods

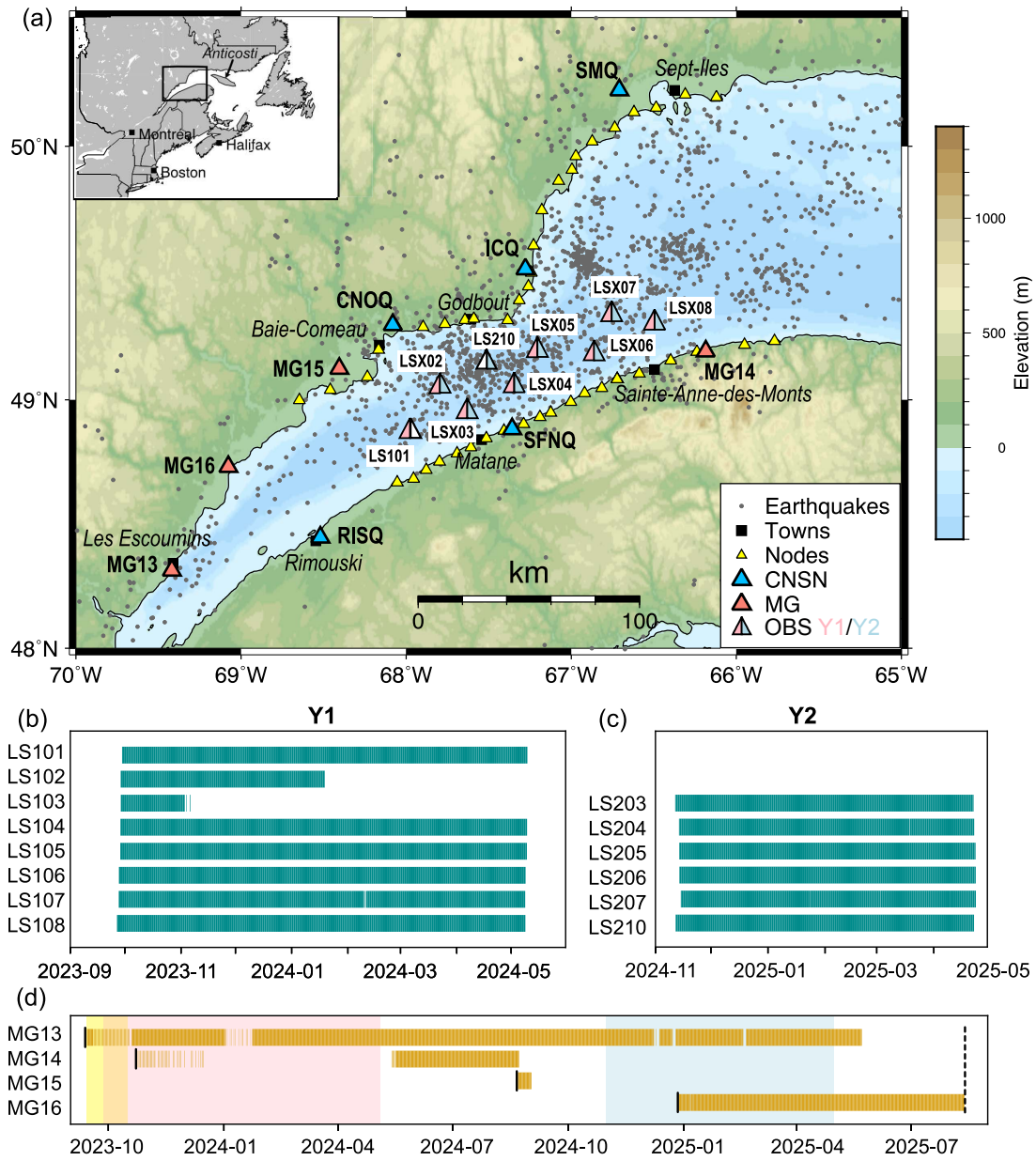

Figure 1 (a) Earthquake and LSLS Amphibious Seismic Network station distributions and (b-d) data availability. Earthquake catalog is from NEDB (NRCan, 1985), 2000-2023. Offshore stations include 8 broadband OBS (Y1: September 2023 to May 2024; Y2: November 2024 to April 2025). Y1 sites: LS101-108; Y2 sites: LS202-208 and LS210. Site labels "LSX0N" denote common sites occupied in Y1 and Y2 (X=1 and 2, N=2 to 8). LS101 in Y1 only; LS210 in Y2 only. In addition to 5 Canadian National Seismograph Network (CNSN) stations, land stations include 4 McGill stations (MG13-16) with various start dates (black short vertical lines in (d)), and 48 short-period nodal sensors (September - October 2023) along both shorelines. The most recent data collection to MG sites was in August 2025 (black long vertical dashed line). The operation periods of the nodal array and the OBS Y1 and Y2 experiments are marked in (d) with yellow, pink and blue background shades, respectively.

and drop sites were chosen to minimize potential overlap with time windows and areas of intense commercial fishing activities that could have inadvertently interrupted the recording or damaged the instruments. We also deployed 48 SmartSolo 3C nodal sensors along the north and south shorelines (24 sensors on each side) for about a month from September to October 2023. The exact operation periods of individual nodal sensors were dictated by the battery life of the instrument. In addition, we installed 4 broadband land stations (MG13, MG15, and MG16 on the north shore, MG14 on the south shore) to complement the coverage of CNSN stations in this region. The distribution of all types of stations is shown in Figure 1; station coordinates and other information are in Supplementary Table S1.

2.1 Offshore deployment

The offshore component of the network consisted of two OBS deployments, the first spanning September 2023 to May 2024 (Year 1, Y1) and the second spanning November 2024 to April 2025 (Year 2, Y2), covering

the same region. The instruments were Güralp Aquarius broadband OBSs from the Canadian OBS instrument pool at the *National Facility for Seismological Investigation* (NFSI). As the NFSI was still in the process of accruing its instrument fleet at the time of the Y1 deployment, the project also served as an instrument verification field test. Each NFSI Aquarius OBS is equipped with a broadband triaxial force-feedback sensor with a flat response from 120 seconds to 100 Hz. The OBS unit also includes an absolute pressure gauge (Keller PA-10L) and a High-Tech HTI-04-PCA/ULF hydrophone with passband 100 seconds to 8 kHz, although not all instruments were equipped with these at the time of the deployment. The sampling rate for the seismic channels was set at 250 Hz. A sampling rate of 1 kHz is anticipated in the future for the hydrophones in order to record higher-frequency whale calls, including some sei, humpback, and North Atlantic Right Whale calls (Baumgartner et al., 2008; Kowarski et al., 2019; Simard et al., 2019), but it was limited to 100 Hz by firmware at the time of this project.

The unique LSLS geographic setting allowed us to rent a small fishing boat with adequate deck space to carry out the deployment and recovery (Figure 2a). Y1 deployment had been planned to start from Matane and proceed downstream, finishing near Sainte-Anne-des-Monts (SAdM) (Figure 1). Operations were to be carried out daytime-only, averaging 2 to 3 OBSs per day and docking overnight at ports of opportunity from where the crew and science party were to be shuttled to local hotels/inns. This plan proved significantly more economical than contracting a larger research vessel, despite time lost transiting to/from ports and limiting work to daylight hours. However, it was also more susceptible to weather conditions. As the science and tech team prepared for the deployment in mid-September, Hurricane Lee swept through the Maritimes and the Gulf of St. Lawrence, which in coincidence with other logistical challenges led to a last-minute vessel change and a revamp of the mobilization plan. The deployment consequently started from SAdM and proceeded upstream to Matane. The recovery cruise was also carried out by a local fishing vessel in a similar manner.

A total of nine OBSs (LS101-109) were dropped between September 26 and 29, 2023 in Y1 experiment, but one unit (LS109) surfaced shortly after deployment due to electronic problems, and was shipped back to NFSI for examination. Therefore, the Y1 deployment consisted of eight OBS (LS101-108) (Figure 1b). LS102 surfaced prematurely on April 5, 2024, shortly before the rest of the group (LS101, 103-108) was recovered between May 8 and 9, 2024. LS102 was eventually reported found on the south shore, near the town of Gaspé, and was recovered by the NFSI in November 2024 during the Y2 deployment operation. Subsequent analysis indicated that LS102 had surfaced due to low-level water ingress through one of the electrical connectors, triggering the release circuit. LS103 only recorded data for approximately 6 weeks (September 28 to November 7, 2023) due to an internal malfunction. This malfunction also prohibited measurement of the final clock drift and tilt reading during instrument recovery.

Deployment and recovery cruises in Y2 again used a small, local fishing vessel. Deployment took place on November 11 and 13-14, 2024, with high winds prohibiting work on November 12 (although this provided time to collect the drifter LS102 from Gaspé). Nine instruments were originally deployed (LS201-208, LS210). During the deployment, LS201 would not communicate with the acoustic transponder once in the water. It was recovered when it resurfaced after the backup timer (pre-set to be an hour upon arrival on the seafloor) triggered release. This issue was determined to be a loose transponder connection that could not be fixed in the field, so redeployment was not attempted. Therefore, the Y2 deployment also consisted of eight OBS (LS202-208, LS210), with seven sites (LS202-208) reoccupying the Y1 sites LS102-108 (Figure 1). LS208 surfaced prematurely in February 2025. It was tracked via GPS for about 2 weeks as it drifted downstream, before signal was lost slightly offshore of Les-Îles-de-la-Madeleine. The NFSI attempted public outreach via social media to find out if it had been seen, but there were no positive responses and it is considered lost. During the recovery cruise, communication was established with LS202 and instrument status readings were normal, but the power level when the burnwire was activated was unusually low and the instrument failed to release despite repeated attempts. The location of this station near the outlet of a river suggests that sediment deposition on the burnwire assembly may have caused the release failure. The recovery attempt had to be abandoned, although the OBS was instructed to run the burn circuit indefinitely. We have no evidence that it has surfaced to date. Six of the seven remaining OBSs (LS203-207, LS210) were recovered successfully on on April 22 and 23, 2025 (Figure 1c).

2.2 Onshore deployment

As of the start of our experiment, Natural Resources Canada (NRCan) operated 5 CNSN broadband seismometers in the Lower St. Lawrence region for seismicity monitoring (Figure 1). However, with only three stations on the north shore and two on the south shore, the average inter-station distance was over 100 km, making precise earthquake location and subsequent source parameter inversion challenging. We complemented the land seismic network by installing 48 nodal sensors (24 along each shoreline) and 4 broadband stations on the north and south shores (Figure 1). Station coordinates and operation periods are listed in Supplementary Table S1.

We used the SmartSolo IGU-16HR 3-Component nodal seismic acquisition system for the nodal array deployment (Figure 2c). These stand-alone seismometers include sensors at a natural frequency of 5 Hz, 64 GB data storage, and a battery life of $\sim$ 30 days if sampling continuously at 250 Hz. The light weight (2.4 kg) and small footprint (103mm(L) × 95mm(W) × 187mm(H) w/o spike) make them user-friendly and cost-effective options for temporary deployment of a large number of nodes. The inter-station distance of the LSLS-ASN nodal sensors was designed to be $\sim$10 km, mainly dictated by the number of available nodes and the length of shorelines to cover. However, due to topography and road ac-

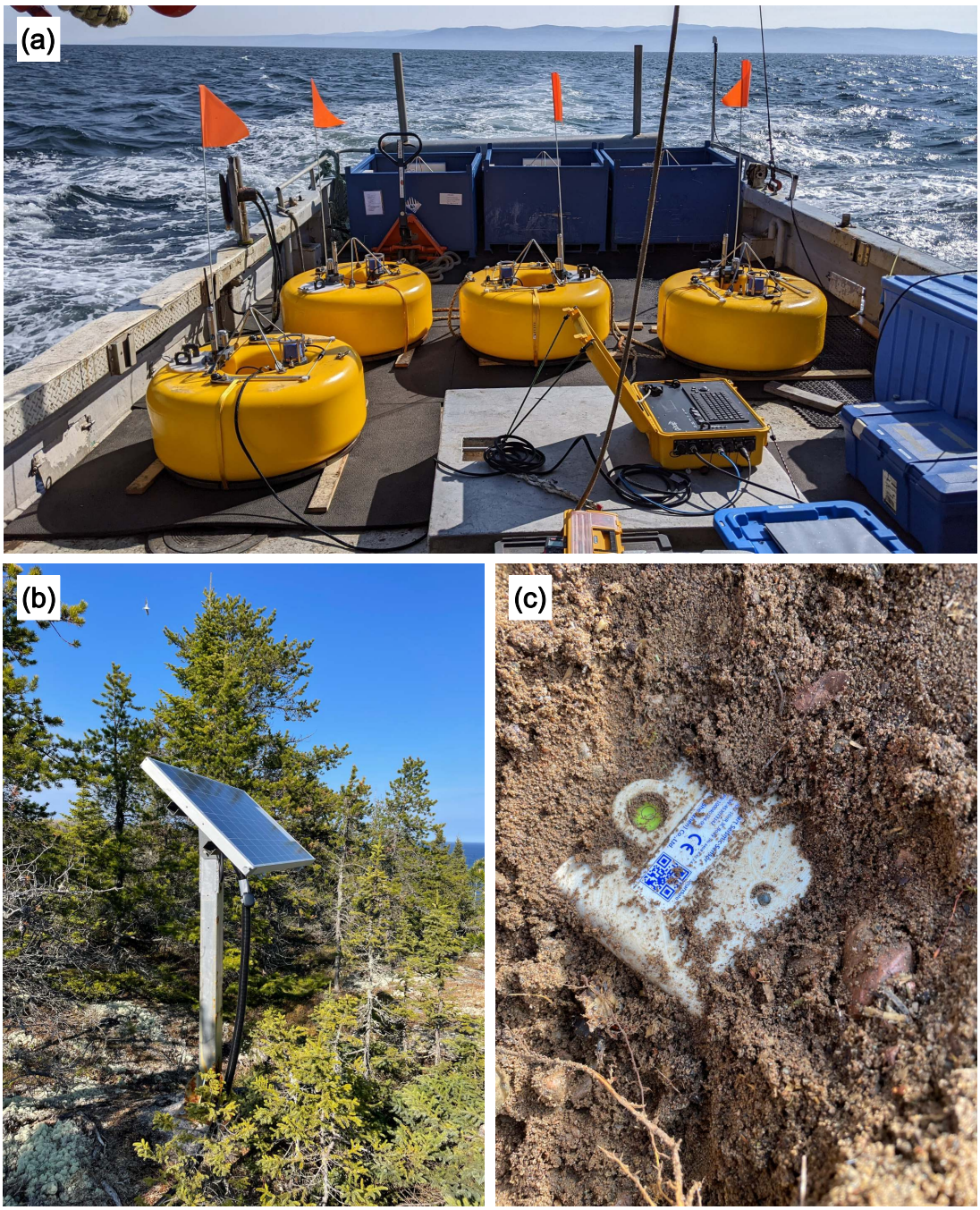

Figure 2 Field photos of different types of seismic stations/sensors deployed in the LSLS experiment. (a) Four NFSI Guralp Aquarius OBS units loaded on *Kalynic*, a fishing vessel operated by Pêcherie Henry for Y1 deployment. (b) Solar panel, pole and cable connection of MG13 at Les Escoumins. (c) A SmartSolo nodal sensor buried in the ground.

cess variability the actual distance varied from ∼10 to 20 km. The two lines of arrays still effectively covered the shorelines of the Lower St. Lawrence Seismic Zone (Figure 1). The nodal array operation period was about a month from mid-September to mid-October 2023.

We also installed four broadband seismometers in conjunction with the OBS deployments, at Les Escoumins (MG13), Cap-au-Renard (MG14), Chute-aux-Outardes (MG15), and Forestville (MG16) (Figure 1). Due to land access and instrument availability issues, these stations started operation at different times in 2023-2024, and therefore have various temporal overlaps with the Y1 and Y2 OBS experiments (Figure 1d). MG13 occupies the former CNSN site LESQ at the Marine Environment Discovery Center of Parks Canada in Les Escoumins (Figure 2b). MG14 and MG15 are located on private properties, while MG16 is on municipality land provided by the Forestville City Council. MG13-15 have Nanometrics Trillium Compact Posthole sensors (20 s to 100 Hz), whereas MG16 has a Guralp CMG-3ESP sensor (100 s to 50 Hz). All MG stations include a Centaur data logger and are powered by solar panels on site. Sampling rate is set at 100 Hz at MG13-15, 50 Hz at MG16.

2.3 Data coverage

The 2023-24 (Y1) LSLS-ASN experiment collected a data set that includes ∼8 months of the OBS network (September 2023 to May 2024), 1 month from the nodal

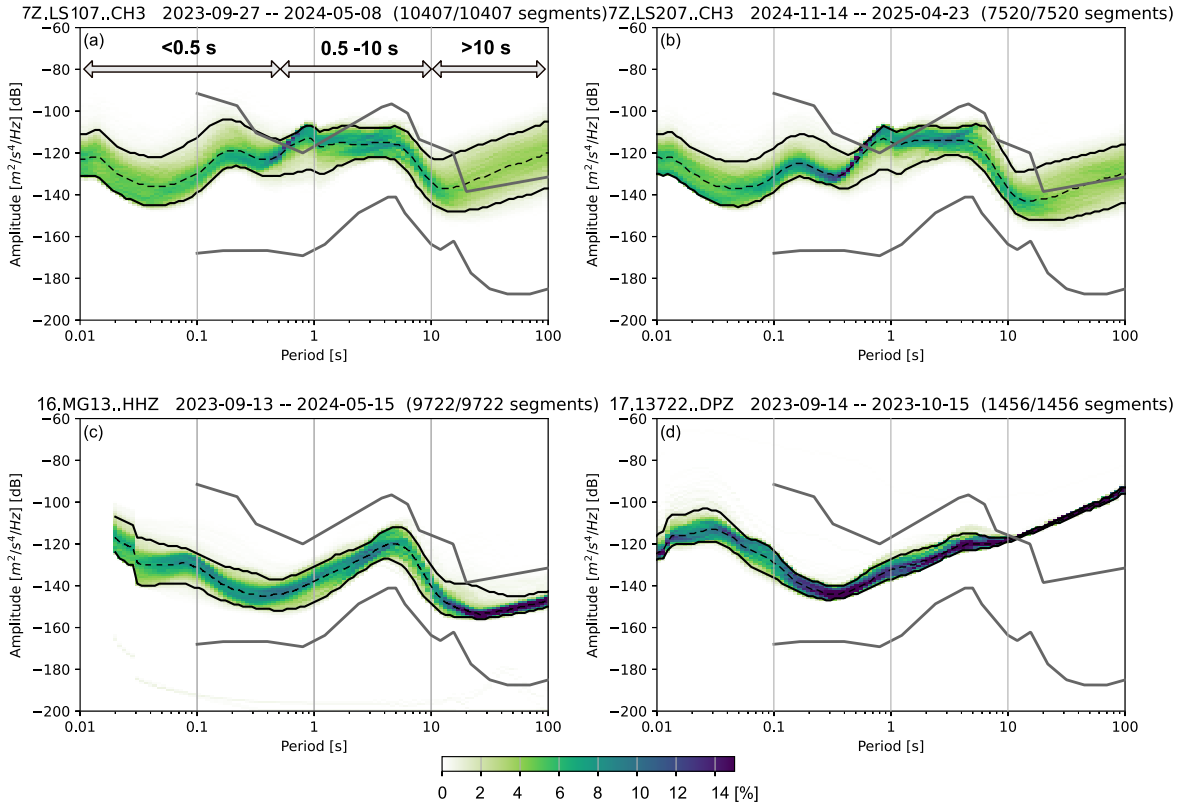

Figure 3 Examples of Probabilistic Power Spectral Densities (PPSD) of vertical (CH3/Z) components at a) Y1 OBS LS107, b) Y2 OBS LS207 (which reoccupied the LS107 site), c) land station MG13, and d) North Shore nodal sensor N06. Solid black lines represent the 95 (top) and 5 (bottom) percentiles, and dashed lines represent the medians. Note that different data periods and sampling rates, hence data segments, are used in each PPSD calculation. Dark gray lines are the NHNL and NLNL from McNamara and Buland (2004). Double-headed arrows in (a) mark the three frequency bands within which the average power amplitudes are shown in Figure 4.

arrays (September to October 2023), and variable operation periods of the MG stations. The 2024-2025 (Y2) experiment collected ∼6 months of the OBSs (November 2024 to April 2025) and various periods of the MG stations. All CNSN stations in this region operated continuously throughout the period. Figure 1b-d shows the data availability chart for both Y1 and Y2 experiments.

Of the eight OBSs deployed in Y1, six (LS101, LS104-108) had near 100% data return rates. Of the eight Y2 OBSs deployed in Y2, six (LS203-207, LS210) were recovered in April 2025 with 100% data return rates. LS102, LS103, LS202, LS208 had zero to partial data coverage for reasons detailed in Section 2.1.

For the MG stations, MG13 and MG16 had complete to near complete data coverage from their respective deployment dates (MG13 in September 2023, MG16 in December 2024) to the last data retrieval in August 2025 (Figure 1d). However, the Guralp CMG-3ESP sensor and the Nanometrics Centaur digitizer at MG16 appear to have been configured inconsistently. This mismatch likely caused problems with the instrument response files and prevented us from using the data in this report. Power issues including power controller malfunction and solar panel damage at MG14 and MG15 resulted in significant data gaps (Figure 1d). MG14 had ∼3 months of continuous data before operation stopped in August 2024. MG13, 15, and 16 were retrofit in August 2025 and continue to operate as of writing of this report. Noise analysis results of MG stations in Section 3 are thus based on data from MG13 and MG14.

All 48 nodal sensors had complete data recovery for about 30 days from September 14 to October 15, 2024. The start/end dates of each nodal site vary by ±1-2 days (Supplementary Table S2).

2.4 OBS data preprocessing

Clock drift correction was applied by assuming a linear drift throughout the recording period for OBS stations with valid final clock offset measurements (Table S1). For Y1, final clock offsets could not be obtained for stations LS102 due to complete battery drainage and instrument shutdown hence loss of time recording prior to recovery, LS103 due to an internal components communication problem which prevented data recording to the long-term storage, and LS107 due to a hardware reboot which prevented the measurement of the final clock offset. For Y2, final clock offset measurements were made for all six recovered stations (LS203-207 and LS201; Table S1). Both Y1 and Y2 clock offset measurements (on deck) showed a distribution skewed toward a negative offset (OBS clock slower than real GPS time). The highest drifts were observed in Y1 at station LS106 (-6.3 ms/-day, in absolute values greater than 4 ms/day, which is equivalently 1 sample point at 250 Hz sampling rate), and in Y2 at station LS207 (-3.1 ms/day).

Orientations of the seismometer channels were not

determined in the NFSI data preprocessing step. Channels CH1 and CH2 are nominally horizontal, oriented as North and East respectively in the instrument's internal reference frame. CH3 is nominally vertical. A measurement from the on-board MEMS accelerometer taken shortly before release was used to estimate the tilt axis orientation at deployment and/or recovery for each instrument (Table S1). In Y1, tilt was not measured at deployment for stations LS106 and LS107, nor at recovery for stations LS102 and LS103 due to instrument issues described above. In Y2, tilt measurements were obtained for all stations at deployment, and all stations except LS208 at recovery. Of the tilt measurements which were collected, the maximum estimated tilt angle from vertical in each year's deployment is $3.65°$ at LS107 and $1.8°$ at LS207.

3 Noise analysis

Ocean bottom seismometer recordings are inevitably imprinted by a variety of environmental (ambient) noise and possibly instrumental noise; both types of noise can be site specific. Before using the OBS data for earthquake detection and source parameter inversion, we need to quantify the ambient noise levels, and analyze and distinguish the noise sources. We first calculate the Probabilistic Power Spectral Density (PPSD; McNamara and Buland, 2004) for all available data (onshore and offshore) to get a global view of the noise levels and spectral distribution.

Figure 3 shows examples of PPSD of the vertical (CH3) components at two OBS stations at a common (reoccupied) site (LS107 and LS207), a land broadband station (MG13) and a nodal sensor (N06). Overall the power density distribution at each station closely tracks the New High Noise Level (NHNL) and New Low Noise Level (NLNL) defined by McNamara and Buland (2004) between periods 0.1 and ∼10 s. The OBS noise levels are at or slightly above the NHNL for periods longer than ∼20 s. OBS noise level is also in general higher than the land stations across the spectra. While the nodal sensors have an instrument natural frequency of 5 Hz, we observe at many nodal sites noise levels comparable to that of the broadband stations up to ∼5 s period, as shown by an example at the north shore site N06 in Figure 3d.

Figure 4 shows the average power amplitudes at each component of each station in short (<0.5 s), intermediate (0.5–10 s), and long (>10 s) periods, projected along a profile parallel to the St. Lawrence River with LS101 as the starting point. The land stations MG13 and MG14 have overall the lowest noise level across the board. The OBS sites exhibit consistent noise levels at reoccupied sites, with the exception of a few sites for the CH3 component in the >10 s period range. Within the <0.5 s period range, OBS stations have comparable noise levels in all three components, which are in general lower than those of the nodal sensors. There appears to be a decreasing trend of the average noise amplitude toward the downstream direction, although the total variation is only about 20 dB across ∼200 km along the river. The north shore sensors generally recorded higher noise levels than those along the south shore within this period range, in particular N14-N25 downstream, which could be due to passing traffic (typically, 0.05 to 0.2 s) and/or sensor/ground coupling issues (a couple of high noise nodes were found at the time of instrument recovery in sandy soil loosened probably by precipitation). Within the 0.5 to 10 s period range, the downstream decreasing trend in the OBS noise amplitude seems to persist for the two horizontal components, but is not visible for the vertical component. Nodal sensor noise levels are consistently lower than on OBSs, except for the last 5–6 sites downstream along the north shore (Figure 4; Figure S1). The low noise level beyond the instrument natural frequency of 5 Hz renders the seismic nodes a useful dataset for the LSLS small-to-moderate magnitude earthquake source parameter analysis. Within the >10 s period range, OBS stations have the highest noise amplitudes at the horizontal components, which, as will be discussed in the following, most likely reflect the tidal effects. As expected due to their 5 Hz natural frequency, nodal sensors also have very high noise levels and are effectively not usable for this long period range.

Below we discuss the power density characteristics and possible sources.

3.1 Microseisms

Microseism peaks are generally widespread and recognizable in the broadband seismic noise spectrum in two frequency ranges. The single-frequency, or primary, microseism peak has lower amplitude and longer period (T = 10–16 s), generated in shallow coastal waters through vertical water pressure variation or from waves crashing onshore (Hasselmann, 1963). The higher amplitude and shorter period (T = 4–6 s) double-frequency, or secondary, peak is generated by the superposition of opposing ocean waves that impose pressure perturbation in the water column transmitted through the solid Earth (Longuet-Higgens, 1950). In the aggregated and median PPSD plots (Figures 3 and 5), the double-frequency (secondary) peak is clearly observed across all the stations. However the single-frequency (primary) microseism peak does not stand out for the OBS recordings. The noise amplitude of the horizontal components is already higher than the NHNL in the 10–16 s range (Figure 5). The vertical component has overall lower amplitudes in this period range but does not show a clear primary microseism peak, probably due to the smearing from the aggregation and average over ∼10,000 data segments spanning the entire experiment. The spectral distribution using a shorter duration (1-hour) of Y1 data does exhibit the primary microseism peak on the vertical component CH3, with the amplitudes more pronounced at the downstream stations LS106, 107, 108 but less so at the upstream stations (Figure S2). This along-stream distinction suggests the St. Lawrence inland seaway environment may also play a role — the downstream stations are likely more impacted by the open ocean conditions hence producing more visible primary microseism peaks. The lack of a clear primary microseism peak is also reported for the

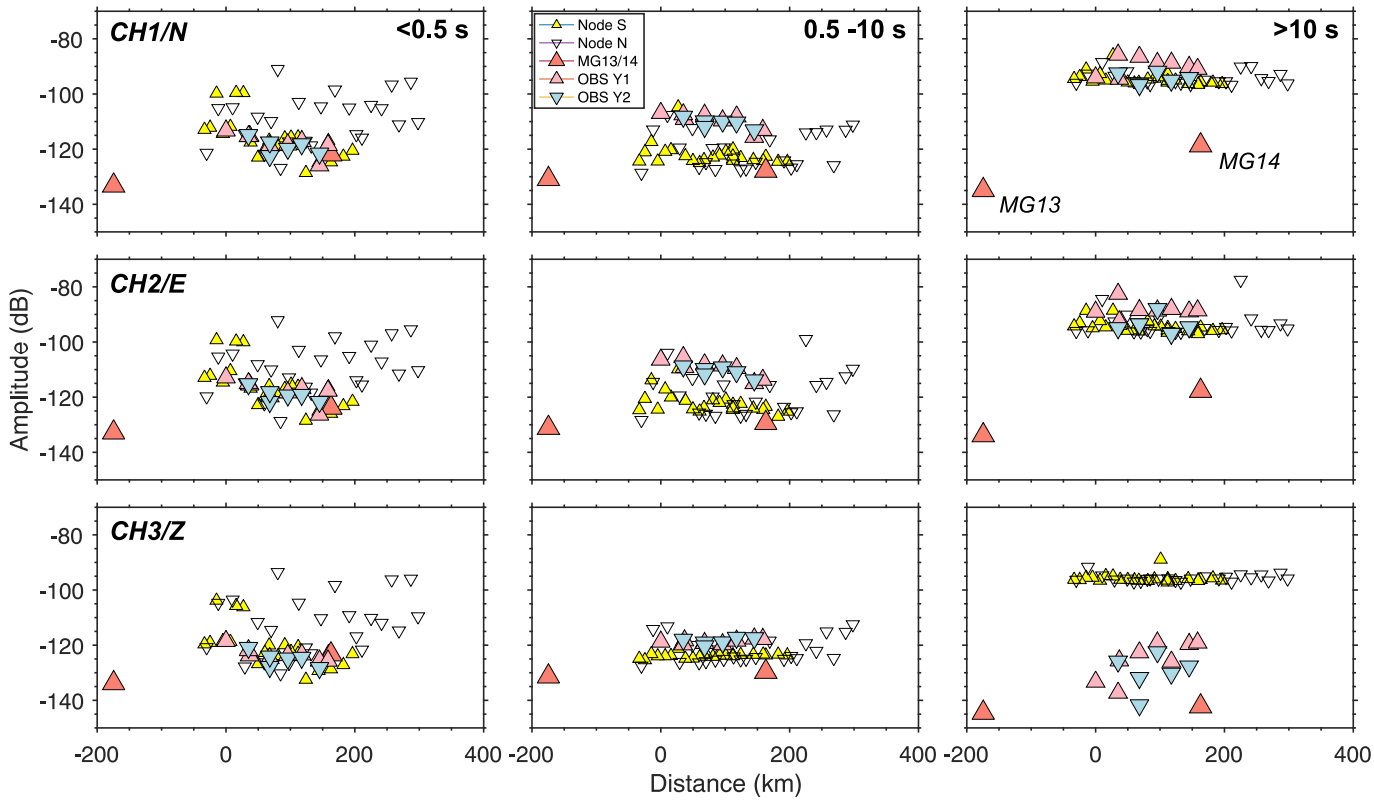

Figure 4 Average power amplitude on three components (from top to bottom: CH1/N, CH2/E, CH3/Z) of all OBSs, nodal sensors, MG13, and MG14 for period ranges: (left) <0.5 s, (middle) 0.5 to 10 s, and (right) >10 s. Distance is projected along a profile approximately along the river, with the starting point at LS101 and ending point at (lon, lat) = (-64.803, 50.077). Distance increases along the downstream direction. MG13 and MG14 are upstream and downstream of LS101, respectively.

aggregated PPSDs from an OBS experiment in the Red Sea (Parisi et al., 2024), a similar sea inlet environment as LSLS.

3.2 Water flow and tidal noise

Median levels of the vertical component PPSDs of the OBSs are similar to those at the land station (MG13) at periods <0.1 s (frequencies >10 Hz) and in the 5–10 s range, near the double-frequency (secondary) microseism peak (Figures 5c and 5f). However, for periods between 0.1 and ~5 s, as well as >10 s, the OBS are up to 20 dB noisier. This effect is more pronounced on horizontal OBS channels, which are notably noisier than MG13/14 even at 5–10 s periods, and are up to 40 dB noisier than MG13/14 at long periods (>10 s; Figures 5a-b, 5d-e). After the Y1 deployment, we hypothesized that the peak noise levels, particularly on the horizontal components at ~0.5 to 2 s, were amplified by the flags that were attached to the OBS units for easy identification on the water surface during the recovery operation (see Figure 2a), which could potentially flap in a bottom current. Therefore, as a test and precaution, we removed the identification flags from all the OBS units in the Y2 experiment. However, this high-noise band persisted; it does not appear that the flags contributed significantly to noise levels. This leads us to hypothesize that the high noise levels on the OBS horizontal components between ~0.5 and 2 s probably reflect the water currents on the riverbed.

We observe a systematic decrease in the period of the peak power (median values) on the horizontal components (CH1/N and CH2/E) from ~2 s at the most upstream station LS101 to ~0.5 s at the most downstream station LS108 (Figures 5a-b). The same along-river systematic shift is also observed from the Y2 data, again from ~2 s at the most upstream station LS203 to ~0.8 s at the most downstream station LS207 (Figures 5d-e). A closer examination of the PPSDs of selected one-hour long waveforms showed that the frequency shift occurs synchronously across all three components, albeit at lower amplitudes for the vertical component (Figure S2), which explains why the peak power frequency shift is not as clearly observed in the vertical component (CH3/Z) of the median PPSDs (Figure 5c and 5f) and suggests a primary source from horizontal ocean currents.

We further hypothesize that daily tides may modulate the noise fluctuation at the >10 s period range. In an estuary setting, the tidal wave movement exhibits a stronger impact on the riverbed in the lateral direction, which may explain the higher noise amplitudes observed at the OBS horizontal components at periods >10 s (Figures 4 and 5). The tidally driven water flow can be further quantified to be proportional to the time derivative of the tidal height (H). Figure 6b shows the spectrogram and power amplitudes averaged over long (50–200 s) and short (2–10 Hz) period ranges at LS106, and the predicted tidal wave heights at the nearest town Sainte-Anne-des-Monts (15-minute tide prediction data downloaded from https://tides.gc.ca/en/stations). Both the long- and short-period amplitudes exhibit clear tem-

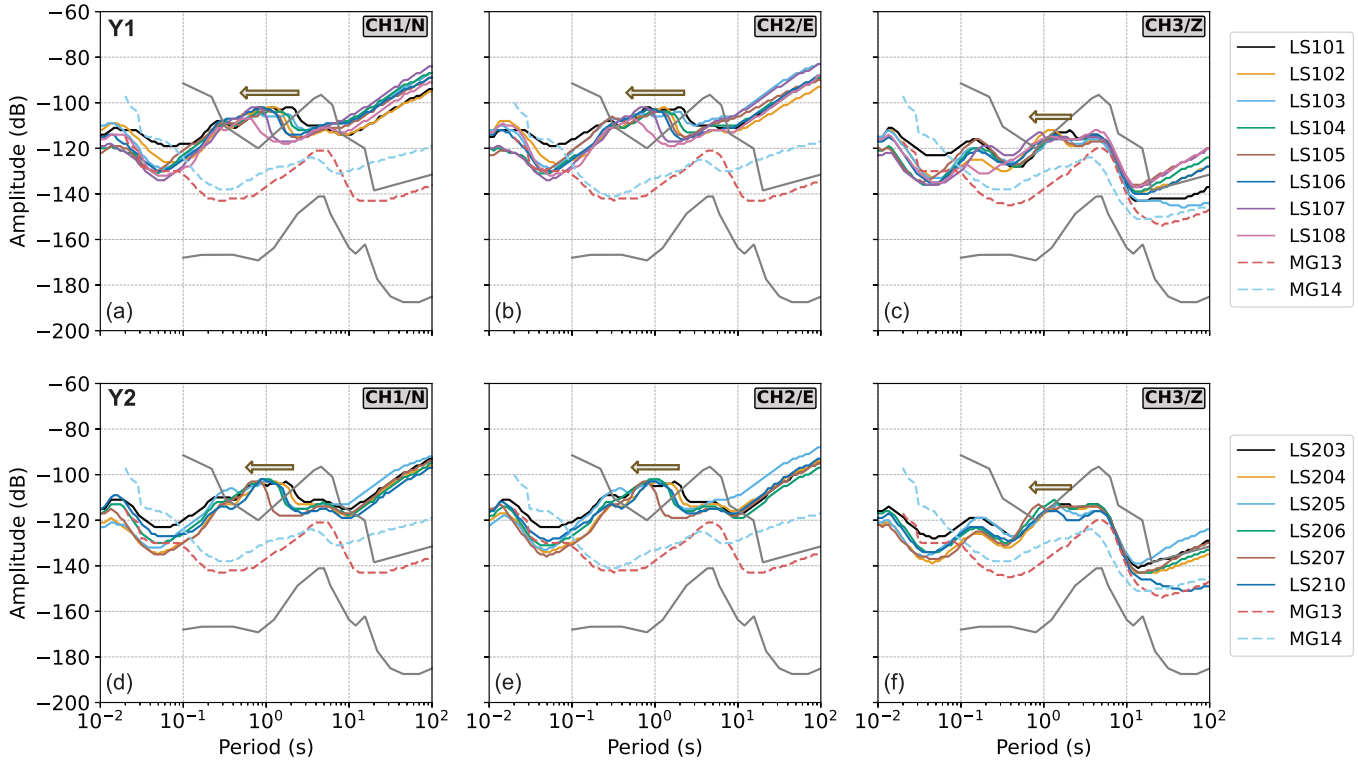

Figure 5 Median PPSDs of (a-c) Y1 OBS LS101-108 and (d-f) Y2 OBS LS203-207, LS210 (solid color lines). Median PPSDs of land stations MG13 and MG14 (dashed lines) are plotted for comparison. Gray lines are NHNL and NLNL (McNamara and Buland, 2004). Arrows in each subplot mark the frequency shift in the peak power from upstream to downstream OBSs.

poral correlations with dH/dt, which is also observed to various degrees from the limited time periods we examined at LSL106 (Figure 6b, Figure S3) and LSL103 (Figure S3). The responses at multiple periods may result from the coupling between tidal forcing and a variety of fluvial processes such as turbulent water flow, bedload transport and geomorphic irregularities (Govi et al., 1993; Burtin et al., 2008; Schmandt et al., 2013).

3.3 Traffic noise

Most LSLS land stations (MG and the nodal sites) recorded daily and weekly noise level cycles at the short period range, for example, 4–14 Hz, that reflects cultural noise from traffic and other human activities (Figure 6a).

For the offshore stations, vessel traffic noise may also play a role. Modern commercial ships usually generate noise in the frequency range of roughly 20 to 500 Hz, and the noise level is dependent on the ship-to-receiver distance (McKenna et al., 2013). Even in the absence of a nearby ship, the background sound level can be dominated by noise from distant ships because the 20–500 Hz acoustic waves can travel long distances underwater. A recent study also showed small vessels, such as sailboats, yachts, tour boats and ferries, could radiate underwater noise comparable to larger commercial vessels (Shipton et al., 2025). Therefore, it is possible that some of the high-frequency noise recorded by the OBS stations is sourced from the marine traffic along the estuary. Analysis of a randomly selected 24-hour waveform record at station LS108 reveals an abundance of high-frequency energy bands extending up to the Nyquist frequency of 125 Hz (Figure S4). Each high-frequency energy burst persists for approximately half to one hour, with the associated harmonics exhibiting characteristic Doppler frequency shifts and Lloyd's mirror effect arising from multipath interference (Figure S5). These features are diagnostic signatures of passing ships, indicating that the observed high-frequency energy bursts are attributable to ship noise (Barlett and Wilson, 2002).

We also observe temporal fluctuations of noise in the 20–100 Hz frequency band (Figure S6) but no clear daily or monthly variations (Figure S7). The lack of obvious monthly variation in high-frequency potentially marine traffic noise level is expected as both the Y1 and Y2 experiments were designed to avoid the active fishing seasons in the estuary. Future analysis needs to compare the high-frequency noise variations with detailed marine traffic schedules, in order to attribute them to exact sound sources in the LSLS shipping corridor.

4 Seismic events and whale call detection

4.1 Earthquakes and possible blast events

For an initial assessment of how the increased station coverage can improve seismic event detection in the LSLS region, we processed 1) the first month (October 2023) data of 8 OBS combined with the 3 nearest CNSN stations (CNOQ, ICQ, SFNQ) and our station MG13, and 2) one month (September 14 to October 15, 2023) of

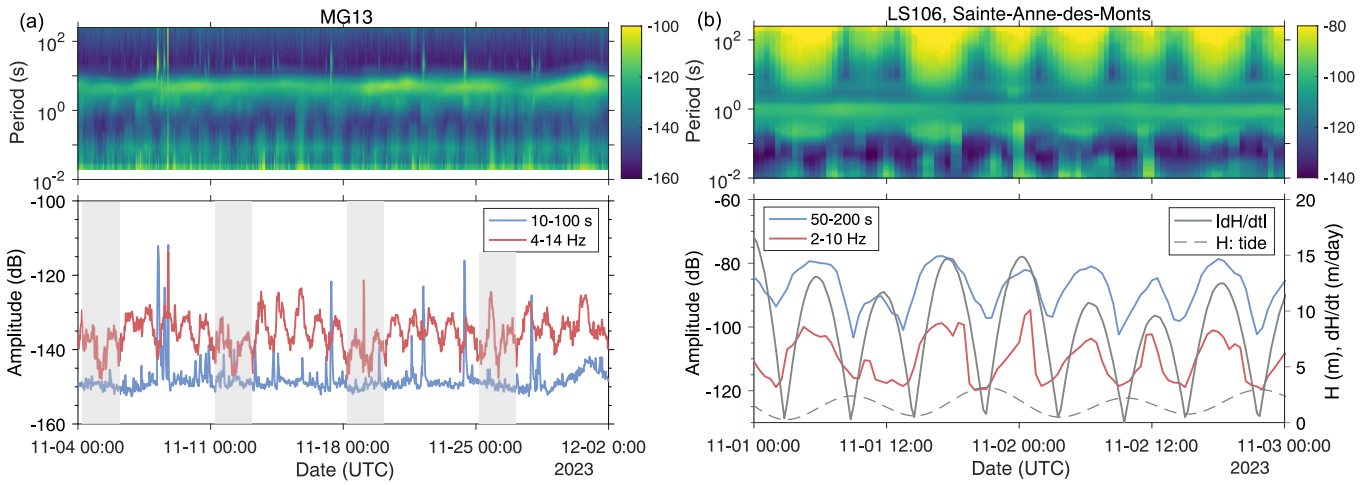

Figure 6 Spectrograms and temporal variations of power amplitudes at selected frequency bands at (a) land station MG13.HHZ, and (b) OBS LS106.CH1. Vertical gray bars in (a) highlight weekends in November 2023. Dashed gray line in (b) shows the tidal height (H in meters) predictions at Sainte-Anne-des-Monts, the closest town to LS106, downloaded from https://tides.gc.ca/en/stations. Solid gray line shows the absolute values of dH/dt; t is time, expressed by date (UTC).

data from the 48 nodal sensors, to create event catalogs for comparison with the NEDB catalog which relies solely on the permanent CNSN stations. We refer to these as the *OBS* and *Nodal array* catalogs in the following, although the OBS catalog did make use of four onshore broadband stations. The objective of creating such initial catalogs in this report is to examine the data quality and confirm that the phase arrivals of small (M ~1) events are indeed visible and usable from the OBS and nodal sensor recordings. We expect to continue refining parameters in the phase-detection and event-association workflow while creating a full earthquake catalog using the combined Y1 and Y2 data.

OBS catalog. We employed the machine learning (ML)-based phase picker EQTransformer (Mousavi et al., 2020), applying a version retrained on global OBS data (OBSTransformer) (Niksejel and Zhang, 2024) to the OBS recordings, and the original EQTransformer model trained on global seismic data (Mousavi et al., 2019) to onshore recordings. We set the P and S phase probability thresholds at 0.1 and the earthquake detection threshold at 0.3 (see Mousavi et al., 2020, for a description of these parameters). Subsequently, we used PyOcto (Münchmeyer, 2024) for phase association, incorporating the velocity model of Plourde and Nedimović (2021) (Table S3). We required a detection to have both P and S picks on at least 2 stations and to have a total of ≥8 picks. This resulted in 420 associations, of which we deemed only 31 to be robust events after visual inspection (vs. eight events reported by the NEDB for the same period, Figure 7). We then relocated events with Hypoinverse (Klein, 2002) and calculated the local magnitude of the event using the Nuttli magnitude (Nuttli, 1973) based on the empirical relation of earthquakes in eastern North America: $M_N = 3.75 + 0.90 \log \Delta + \log(A/T)$, where A is the maximum amplitude, T is the period in seconds and Δ is the distance in degrees. Furthermore, we adopted a magnitude unit correction of +0.11 for events within distances of 10–150 km in eastern Canada as suggested by Bent (2018). Of the 31 hypocenter estimates, 12 are onshore with extremely shallow depths (<3 km, but many <0.1 km; Table S2) and are likely blasts or other industrial activity, rather than earthquakes. Another OBS detection (depth 9.62 km) is also labeled as a blast event in consultation with an internal NRCan blast catalog. We note that three of the eight NEDB events in the October 2023 period were not detected in our preliminary OBS catalog. These include an event of NEDB reported $M_N = 1.71$ on 2023/10/25, which is located more than 100 km north from the nearest station used in detection, and two other events of M_N <1.0, for which we could not visibly identify many phases on the OBS. In summary our OBS catalog detected 18 earthquakes in October 2023, in comparison to eight NEDB events, resulting in >2 times more earthquake detections than the NEDB catalog.

Nodal array catalog. To process the nodal array, we began with the same workflow for EQTransformer and PyOcto, except that, given the increased station density, we opted for a higher minimum number of picks, requiring a detection to have ≥10 total picks and ≥3 stations with both P and S picks. Before proceeding to visual confirmation, we further ran REAL (Zhang et al., 2019) and GaMMA (Zhu et al., 2022) for phase associations, and kept only events detected by all three association algorithms. We then proceeded with the visual inspection, Hypoinverse locations, and Nuttli-magnitude computation. This resulted in 26 detections, including 8 of 10 earthquakes reported in the NEDB during the same period (September 14 to October 15, 2023; Figure 7), eight events we suspect are blasts, and 10 we believe to be previously undetected earthquakes. All the suspected blast events are located on the north shore, mostly in a cluster near Event A (Figure 7a).

Supplementary Table S2 details all three catalogs (NEDB, OBS, nodal array), including 14 events from the NEDB between September 14 and October 31, 2023, with

M_N ranging from 0.75 to 2.34. In the following we highlight two representative events with high number of phase picks from OBS/EQTransformer (marked by stars in Figure 7). Event A on October 10, 2023 is an example of a suspected blast event in both the OBS and Nodal catalogs, with the two epicenter estimates 4.6 km apart (red and cyan stars on the north shore in Figure 7a). Figure 8a shows the P/S phase picks from 120-second waveforms sorted by epicentral distances at all the on- and offshore stations. Despite being more than 50 km north of all the OBS sites, the clear phase arrivals at multiple stations gave a well-constrained epicenter on the north shore which is about 50 km north and south, respectively, of the nearest CNSN stations SMQ and ICQ. Event B is an earthquake that occurred on the south shore on October 28, 2023 with M_N=2.34, listed in the NEDB. All the land and OBS recordings show clear P and S phase arrivals (Figure 8b). Furthermore, its epicenter from the OBS catalog differs from the NEDB by approximately 5 km (black and cyan stars on the south shore in Figure 7a). Event B occurred after the nodal array was decommissioned.

Figure 7c shows our calculated Nuttli magnitudes M_N in comparison with those in the NEDB catalog. Overall the magnitude differences between the common detections from the three catalogs are within 0.5-unit, with the OBS catalog producing generally larger M_N values than the other two. Station-specific magnitude calculations confirmed OBS stations have larger amplitudes, which resulted in larger M_N than the land broadband stations at comparable epicentral distances.

4.2 Whale calls

As a preliminary test of whale call signal quality on the OBS seismic and hydrophone components, we applied the double-spectrogram detection algorithm of Plourde and Nedimović (2022), for whale calls with a regular internote interval (INI), to one month of data from LSL01 targeting both fin whale "20 Hz" calls (Roy et al., 2018) and blue whale A/B notes (Mellinger and Clark, 2003). Other calls without regular INI, such as blue whale "arch" calls, were likely recorded but are not examined in this report.

An example of high-SNR fin whale detection on both sensors is shown in Figure 9a–d. In this case, the spectrogram produced from the seismic data appears almost identical to that produced from the hydrophone, and the measured SNR of the calls match very closely. The median difference of SNR for these 9 calls, $\mathrm{SNR}_{\mathrm{seis}} - \mathrm{SNR}_{\mathrm{hydr}} = 0.1$ dB, and the standard deviation of the difference is 1.2 dB. An example blue whale detection on both sensors is shown in Figure 9e–h. This is again a fairly high-SNR example and again the calls appear very similar on the seismic- and hydrophone-derived spectrograms, with very similar SNR. However, there are other prominent signals present in the seismic data that mask some calls (Figure 9e,g), and that do not appear to be present in the hydrophone data. Supplementary Figures S8 and S9 provide additional plots for these detections that illustrate the detection algorithm.

These two examples demonstrate that the seismic components are about as sensitive as the hydrophone to water-borne signals, at least in this frequency range. The OBS deployed without hydrophones should therefore be almost as capable as those with hydrophones for whale monitoring, even though other seismic signals will sometimes contaminate whale call seismograms. We expect this issue to be more prominent for low frequency whale calls ($\leq$20 Hz) than higher-frequency calls.

We perused seismograms from all 8 OBSs for a selection of fin and blue whale detections; we found that songs could regularly be visually associated across 3 or 4 OBSs, but also frequently only be visible on 1–2 OBSs. More rarely calls appear on 5–6 OBSs, as seen in Figure 10 for a series of blue whale A/B sequences. As LS101 has the earliest arrival time in that example, if we conservatively assume the whale is about halfway between LS101 and LS102, the calls have traveled $\sim$80 km to LS106, where they appear with SNR up to $\sim$7 dB. Note that this song did not get automatically detected as noise levels on other components are comparable to call amplitudes, so SNR was very low on the spectrogram summed from all three components.

5 Discussion

In this paper, we introduce the first amphibious seismic station deployment in the Lower St. Lawrence Seaway with the dual targets of seismicity and marine soundscape monitoring. This report documents data quality, highlights various types of signals (noise), and serves as the foundation for forthcoming projects in seismological, oceanographic, and environmental investigations in the LSLS. Here the distinction between signal and noise is inherently relative: information that constitutes meaningful signal in one project may be regarded as irrelevant or even distracting noise in another. Future efforts in detailed studies of local seismicity, lithospheric structure, marine soundscape, and relation to environmental factors are thus closely intertwined in data processing and results interpretation.

5.1 Possible sources for noise peaks

For local seismicity studies, it is important to consider site effects arising from sediment coverage, instrument coupling, and general environmental factors such as river currents and tidal fluctuations. Sediments on the river bed may impact automated seismic phase detection of arrival times and waveform polarities. Poor coupling with the river bed, due to soft sediments for example, also introduces resonant, tilt, and compliance noise that degrades the signal-to-noise ratio (Crawford and Webb, 2000; Bell et al., 2014; Janiszewski et al., 2019). In particular, the OBS dataset experiences significantly higher noise levels than the land stations (Figures 3 and 5) between 0.1 and 2 s (0.5–10 Hz), which is also the typical frequency range for the source spectra of small-magnitude earthquakes (e.g., M3 and lower) in the Lower St. Lawrence Seismic Zone. Understanding the sources of such noise is thus a prerequisite for proper denoising before earthquake source parameter

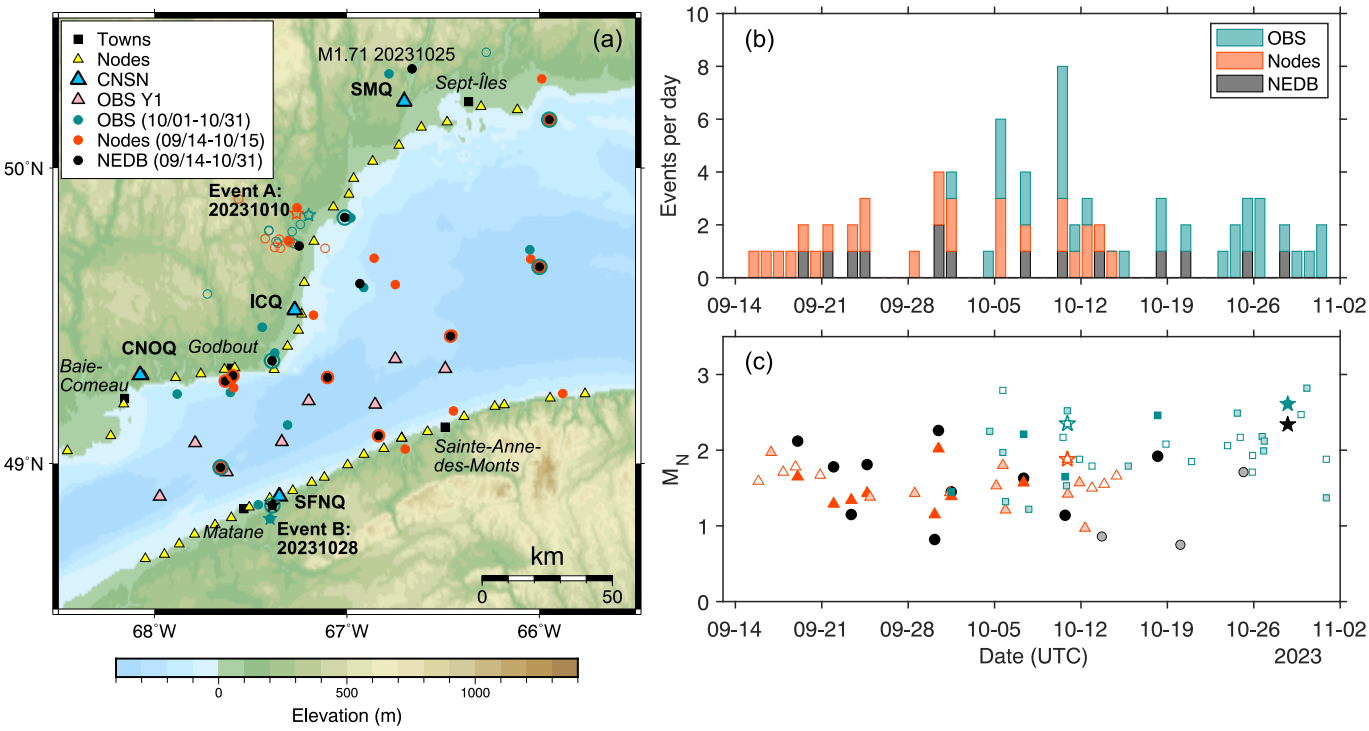

Figure 7 (a) Epicentral distribution of events from the NEDB between 2023/09/14 and 2023/10/31 (14 events, black dots), an enhanced catalog developed using 8 OBSs, 3 CNSN (CNOQ, ICQ, SFNQ) stations, and MG13 for the period of 2023/10/01 to 2023/10/31 (31 events, dark cyan dots), and catalog created using 48 nodal sites between 2023/09/14 and 2023/10/15 (26 events, red dots). Open circles denote suspected blast events in the OBS and nodal catalogs. NEDB epicenters (black) with thick cyan and/or red outlines are those also detected by the OBS and/or nodal catalogs, respectively. Stars: North shore Event A on 2023/10/10 is detected by OBS (M_N=2.35) and nodal arrays (M_N=1.88) but is not in the NEDB; South shore Event B on 2023/10/28 occurred after the decommissioning of the nodal array, is detected by the OBS (M_N=2.61) and also appears in the NEDB (M_N=2.34). (b) Stacked histograms showing the daily number of detected events from the three catalogs, with respective durations marked in Figure 7a legend. (c) Nuttli magnitudes of the three catalogs. Symbols with solid face colors are common detections between NEDB (black circle)/OBS (dark cyan square), NEDB/nodal array (red triangle) catalogs; semi-transparent face colors are non-NEDB-overlap detections; open symbols are suspected blast events; gray circles are three NEDB events missed by the OBS catalog. Stars represent Event A on 2023/10/10 and Event B on 2023/10/28. The NEDB event (solid black circle) on 2023/10/10 has an origin time 17:11:42, different from Event A's origin time at 21:34:44.

inversion studies. The OBS noise within this intermediate period range seems to form at two distinct peaks.

The first peak is centered around 1 s, with a downstream progressive shift in the peak power from period ∼2 s to ∼0.8 s most visible in the horizontal components (Figure 5), and synchronized in the vertical component but at lower amplitudes (Figure S2). This systematic along-stream frequency shift in the 0.8–2 s range is clear evidence of the impact of river currents, which at the regional scale are strongly influenced by the Anticosti Gyre, a persistent cyclonic (counter-clockwise) ocean circulation feature between Anticosti Island and our OBS deployment area (Figure 1). Based on the physical oceanography model by Galbraith et al. (2024), the Anticostic Gyre has the gyre centre located approximately midway between MG14 and Sept-Îles, with a radius of ∼80–100 km, which encompasses the downstream OBS stations. In particular, the ocean current model predicts increasing horizontal velocities 1) from upstream to downstream, 2) from summer (July–September) to winter months (January–March) (Galbraith et al., 2024). Future studies systematically comparing spatiotemporal variations in OBS noise levels with regional ocean current model outputs will be needed to verify the influence of the Anticosti Gyre and elucidate the underlying mechanisms.

The second peak shows consistently at ∼0.1–0.2 s for vertical and 0.2–0.3 s for horizontal components without clear along-stream variation from the time-averaged median PPSDs (Figure 5) nor in the random one-hour data (Figure S2). This shorter-period peak around 0.1–0.3 s (3–10 Hz) may reflect distinct noise sources possibly more sensitive to local site conditions. As noted in Figure 6b, the 2–10 Hz noise level fluctuation also correlates with the rate of tidal height (dH/dt). Such a temporal correlation is also observed, although not as obvious, at other randomly selected time periods or stations (Figure S3). In addition, harmonic tremors from vortex shedding as ocean currents interact with bathymetry irregularities or the OBS instrument itself may also contribute to noise in this frequency range (Essing et al., 2021; Corela et al., 2023), although we have not yet searched for harmonic tremor signals in the LSLS dataset. Our preliminary results are suggestive; full processing of the entire dataset is necessary to validate the identified temporal patterns and definitively attribute them to their causal mechanism(s).

The two distinct peaks both occur at shorter peri-

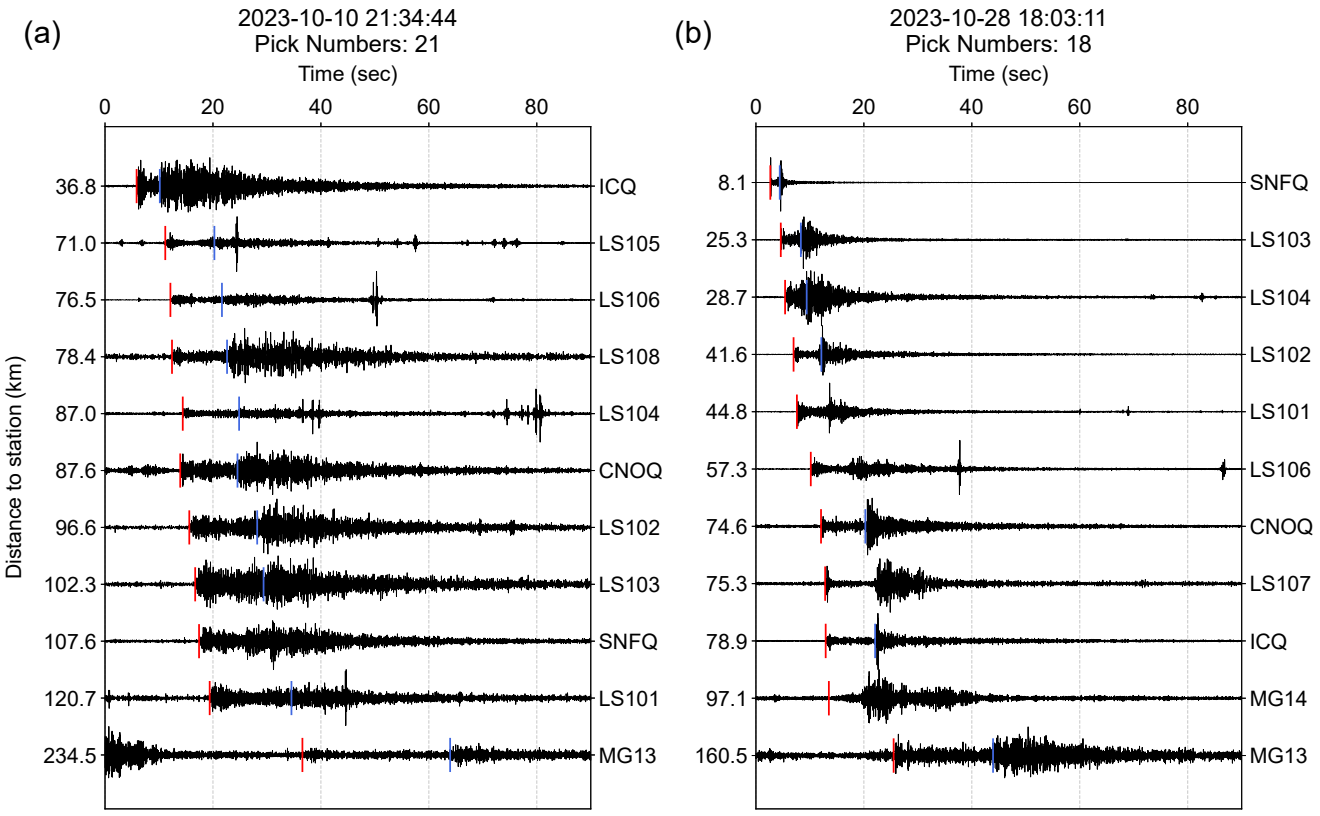

Figure 8 Example normalized waveforms in preliminary OBS broadband station catalog with phase pick detections from the North (or CH1) components, bandpass filtered between 3 and 20 Hz. Red markers indicate P phases, and blue markers indicate S phases. (a) Newly detected Event A on October 10, 2023, (b) Event B on October 28, 2023, previously reported in the NEDB catalog.

ods than the widespread and easily recognizable microseism energy peaks at worldwide broadband stations (McNamara and Buland, 2004). Their presence at OBSs and absence at coastal land stations (see comparison in Figures 3 and 5) supports our interpretation that they source from local sea conditions with rapid energy dissipation inland. Additional amplitude peaks at possible harmonic overtones are also visible, and are more pronounced in the horizontal components, from a random selection of one-hour waveforms in Y1 (Figure S2), which requires detailed analysis in future studies associating these signal/noise ratios to short-time-scale river flow dynamics.

5.2 Uncertainties in seismic events and whale call detections

Many seismic events in the Eastern Canada seismic zones coincide with intensive mining and quarrying operations, with localized blast events (NRCan, 1985), and differentiating these events remains challenging due to sparse seismic station coverage, false detections by the ML phase picker and an incomplete public blasts catalog. For example, both the OBS and nodal array catalogs exhibit a cluster of events on the north shore near the 2023/10/10 Event A (Figure 7a). The public NEDB blast catalog contains no event records during our OBS and nodal array catalog periods (as of writing), but an NRCan internal catalog indicates that this cluster, including Event A, consists of suspected blast events, although the exact source was not confirmed. Event A has a hypocentral depth of 0.06 km and 0.08 km, respectively, from our OBS and nodal array catalogs, with vertical location errors around 1.5 km. It also has notably more prominent surface waves and lower S/P amplitude ratios than the the earthquake Event B (Figure 8). These are all characteristics consistent with a blast source. We are currently working on a ML-based source differentiation algorithm trained on a labeled earthquake and blast event dataset of the Western Quebec Seismic Zone, which can be adapted for the LSLS region for the classification of blast and earthquake sources (Chien and Liu, 2026).

We examined one month of OBS data for fin whale and blue whale (A/B) calls and found it to be a rich dataset. Notably, we found that the seismic components of the OBS appear to be equally sensitive to the whale calls as the hydrophone, meaning the whale-monitoring capability of those deployed without hydrophones is not severely limited. The 250 Hz sample rate of the seismometer (vs. 100 Hz for the hydrophones) allows monitoring for higher-frequency calls such as the blue whale "arch" call, as well as sei whale calls and potentially other species. We found that it was common for fin and blue whale calls to be visible across 3-4 OBSs, which would allow localization via triangulation, but also common for them to only be visible on 1-2 OBSs, meaning that for many calls localization will require in-

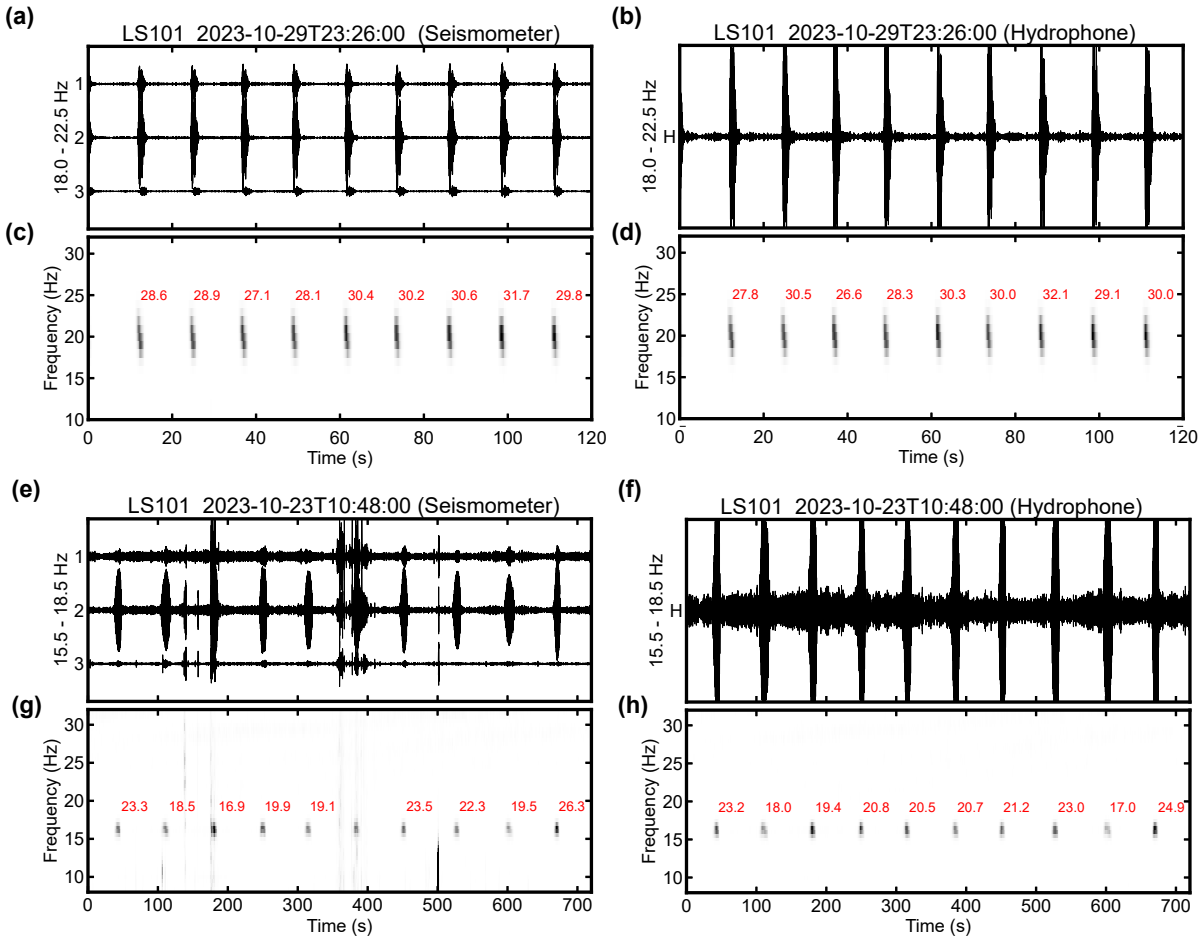

Figure 9 (a-d) Example fin whale detections on LS101 on the seismic and hydrophone channels. (a,b) Two minutes of three-component seismic and hydrophone data, respectively, filtered to the fin whale target band (18.0-22.5 Hz). (c,d) Spectrograms of the seismic and hydrophone data, respectively, with detected calls labeled by their measured SNR in dB. (e-h) As above, but for a blue whale detection in the 15.5-18.5 Hz target band, and using a six-minute window.

corporating estimates of azimuth. Via either method, the OBS data should enable the localization of whale calls and tracking of individual whales in a way that has not been possible with previous hydroacoustic data in the St. Lawrence, which could offer new insights into whale behavior and lead to appropriate conservation measures.

5.3 Future projects using LSLS-ASN data

Correlations between noise levels and environmental time series such as wind speeds and wave heights have already been summarized for datasets from OBSs in deep oceans and on continental slopes (Bromirski et al., 2005; Hilmo and Wilcock, 2020; Zhang et al., 2023). LSLS presents a peculiar marine environment where the seismic waveform data also contain signal/noise specific to the estuary conditions. For example, the steep slopes of the glacially carved riverbed of the St. Lawrence Estuary are favorable sites for submarine landslides and turbidity currents, including earthquake-triggered (Mérindol et al., 2022) and storm-induced turbidites (Normandeau et al., 2020). While turbidity currents are typically associated with slope failures from sediment-rich shelves, the recently observed frequent turbidity current activity near Pointe-des-Monts (PdM) is counterintuitive because of the very limited to non-existent sediment supply from the bedrock-exposed shelf (St-Onge et al., 2011). It also remains unclear whether there are any dynamic triggering effects (e.g., stress perturbation from passing seismic waves, atmospheric pressure fronts) between submarine landslides, turbidity currents, local/global earthquakes, and storms in the LSLS, similar to those documented in the Gulf of Mexico (Fan et al., 2020). Given the dynamic speed (1-2 m/s) and short duration (hours to days) of these landslides and turbidity currents, the local OBS array of LSLS-ASN provides a potential monitoring tool for characterizing the spatiotemporal distribution and relationship between seismicity, turbidity currents, submarine landslides, and storms in the LSLS.

Another St. Lawrence seafloor dynamic process that would be amenable to OBS monitoring is episodic or continuous methane gas seepage, which usually originates from deep reservoirs due to poor sealing of the cap-rock as well as presence of faults or fractures within the reservoir (Embriaco et al., 2014). St-Onge et al. (2011) have mapped more than 2000 pockmarks in the estuary with some active offshore of Matane. While observation and interpretation of gas seepage from seismic data often relies on active-source imaging in hy-

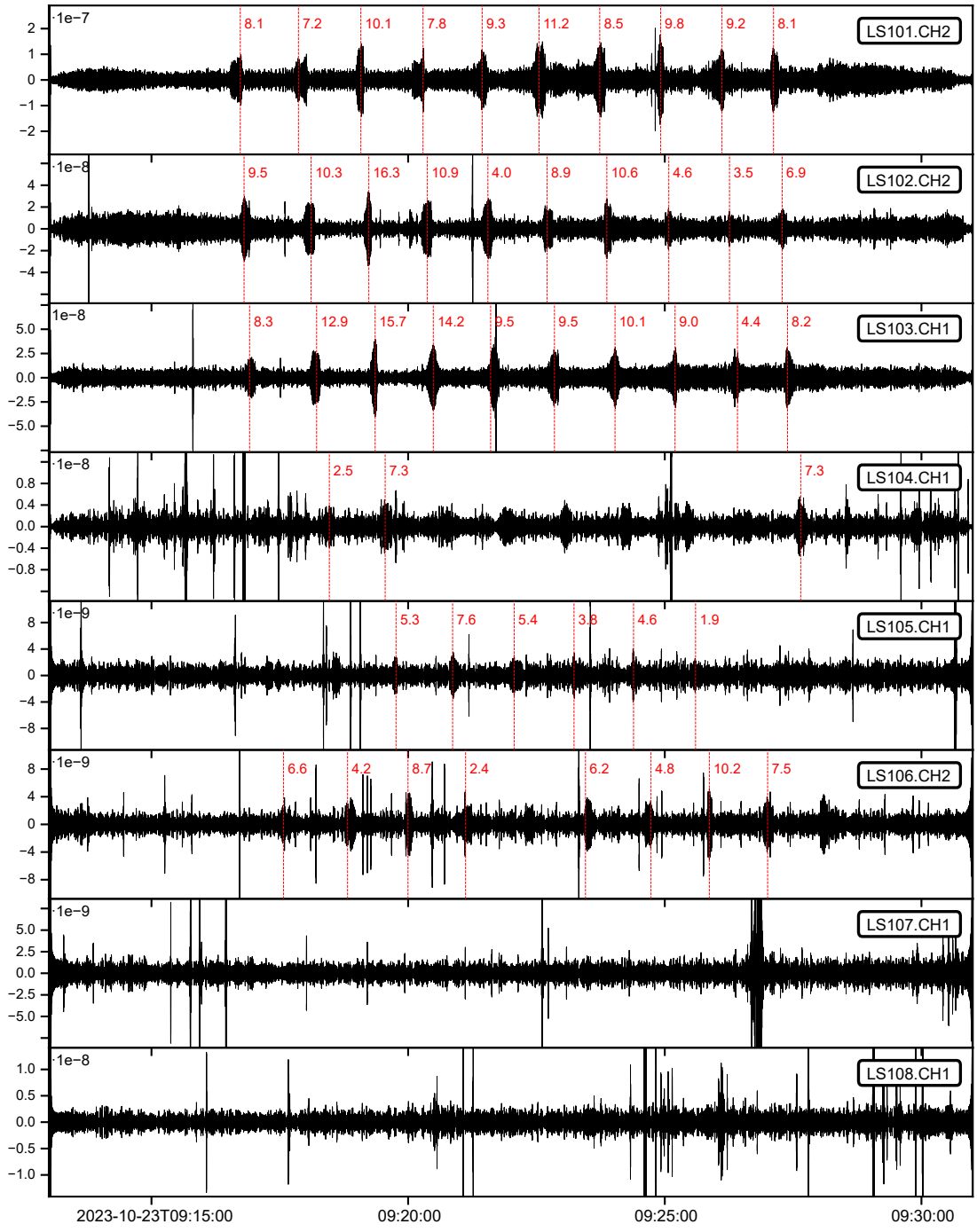

Figure 10 Example blue whale song of A/B sequences captured on six of the eight OBS. The data are all velocity seismograms in m/s. Individual channels with the highest SNR are selected for each OBS, and the detection algorithm was run on only this component to pick call times, which are labeled with their SNR in dB. Some erroneous picks were manually culled from this figure.

drocarbon exploration or scientific geophysical expeditions, it is possible to utilize the whale calls as equivalent active sources to construct seismic records (seismic wave travel-time versus distance) and potentially illuminate structures that interrupt continuous reflection phases (Kuna and Nábělek, 2021), toward a systematic map of gas seepage and improved understanding of slope stability.

The LSLS-ASN network deployment also provides opportunities for studies of lithospheric structure. Both broadband (land and marine) and nodal sensors, if recording global earthquakes with a sufficient signal-to-noise ratio, can provide important datasets for analysis techniques such as receiver functions (RF) that image structural discontinuities in the crust and upper mantle beneath each individual station, with potential for more advanced 2D imaging techniques such as RF common-conversion-point stacking in the case of densely spaced quasi-linear arrays. During the two deployment periods of the OBS network, a total of 98 global earthquakes of magnitude $\geq$6.0 occurred; during the month-long nodal deployment, there were 12 magnitude $\geq$6.0 earth-

quakes worldwide (source: IRIS Earthquake Browser; https://ds.iris.edu/ieb). Taking into account resolution limits imposed by station spacing and network aperture with respect to seismic wavelengths, the geometry of the array will permit detailed modeling of the sedimentary structures and the upper crust using ambient-noise tomography by inter-station cross-correlation.

5.4 Field logistical and operational lessons

As an NFSI pilot project, many aspects of the LSLS OBS experiment were new to our team and differed significantly from cruises on large research vessels for deep water offshore projects that the OBS community commonly undertakes. This presented challenges, but also valuable learning opportunities such as the deployment from a small fishing boat in an estuary environment with tidal currents, instrument mobilization from small fishing ports, marine operation coordination with land support, and the logistical complications of running OBS experiments in the northern Atlantic hurricane season (typically from August to October). For future projects, September operations in Atlantic Canada should be treated as high risk for weather-related delays and include appropriate contingency plans. Our utilization of small fishing boats in the OBS deployment and recovery cruises was operationally flexible and economically affordable, but required careful planning in order to maximize the use of available daylight. Land support was a useful and critical component of the fieldwork. The onshore staff was able to make last-minute accommodation changes and meet the boat at the various ports of opportunity, allowing for much greater flexibility for each daytime OBS operation. Finally, we also found the OBS instrument preparation is best performed in port to the extent possible; such preparation tasks were difficult to perform on the deck of a small vessel due to motion and risk of splashes on sensitive electronic components.

6 Conclusion

The Lower St. Lawrence Seaway encompasses one of the most seismically active zones in eastern Canada and is a critical habitat for marine mammals within a heavily trafficked shipping and fishing corridor. In this report we present the deployment/recovery, data quality and preliminary results from a 2023–2025 amphibious seismic network operated along the LSLS. OBS recordings exhibited elevated noise levels across all frequencies relative to the land-based broadband stations, with particularly pronounced noise between periods of 0.2–2 s and beyond 10 s on the horizontal components. The strong correlation between long-period noise amplitude and tidal cycles points to tidal modulation of riverbed currents as a possible dominant source mechanism. Passing vessel signals are also abundantly recorded, as evidenced by well-defined Doppler frequency shifts and multipath interference signatures. The enhanced seismicity catalog derived from the combined network revealed over two times more earthquakes than reported in the Canadian National Earthquake Database over the first month of deployment, underscoring the capability of dense amphibious arrays to improve earthquake detection in the region. About a third of the OBS and nodal array detections are likely from blasting events on the north shore. Finally, clear detections of fin whale and blue whale vocalizations at multiple OBS sites highlight the potential of this network for passive acoustic monitoring and whale call localization, opening new avenues for integrated geophysical and marine biological research in the LSLS. The LSLS network demonstrates the value of combining offshore and onshore instrumentation for simultaneous geohazard assessment and marine soundscape monitoring.

Acknowledgements

We acknowledge the Canadian Natural Science and Engineering Research Council (NSERC) Ship Time program and National Facility for Seismological Investigation (NFSI) for funding the research vessel time of the 2023-2025 Lower St. Lawrence Ocean Bottom Experiment (LOBEX). OBS instrument operation, maintenance, and data curation is provided by NFSI, which is funded by Canada Foundation for Innovation (CFI). The procurement and maintenance of the nodal seismometers were funded by a CFI grant to Zhang. We also acknowledge support from NSERC Discovery Grants to Liu, Plourde, Darbyshire, Nedimović, and Zhang, and Seed Fund from the Ocean Frontier Institute of Dalhousie University to Zhang and Nedimović. We thank Nicholas Ackerley, Christopher Boucher and Mareike Adam for discussion on the possible blast events and sharing the internal NRCan catalog on suspected blasts in our study area. We thank the Editor and two reviewers, Zoe Krauss and Laura Parisi, for their constructive review comments that helped to improve this manuscript.

Data and code availability

LSLS-ASN OBS data are archived at the NFSI data centre with the International Federation of Digital Seismograph Networks (FDSN) network code 7Z https://doi.org/doi:10.7914/x5w5-z042 (Liu et al., 2023b). Data from land stations (MG13-16 and 48 nodal sensors) will be available through the EarthScope Data Center with FDSN network codes 16 https://doi.org/10.7914/gm3m-q077 (Liu and Harrington, 2015) and 17 https://doi.org/10.7914/tktn-xb44 (Liu et al., 2023a), respectively.

Competing interests

The authors declare no competing interests.

References

Barlett, M. L. and Wilson, G. R. Characteristics of small boat acoustic signatures. *The Journal of the Acoustical Society of America*, 112(5_Supplement):2221–2221, 2002. doi: 10.1121/1.4778778.

Baumgartner, M. F., Van Parijs, S. M., Wenzel, F. W., Tremblay, C. J., Carter Esch, H., and Warde, A. M. Low frequency vocalizations attributed to sei whales (Balaenoptera borealis). *The Journal of the Acoustical Society of America*, 124(2):1339–1349, 2008. doi: 10.1121/1.2945155.

Bell, S. W., Forsyth, D. W., and Ruan, Y. Removing noise from the vertical component records of ocean-bottom seismometers: Results from year one of the Cascadia Initiative. *Bull. seism. Soc. Am.*, 105:300–313, 2014. doi: 10.1785/0120140054.

Bent, A. L. Magnitudes at close and very close distances in Eastern Canada: issues and recommendations. *Geological Survey of Canada*, Open File 8232:32 p., 2018. doi: 10.4095/308131.

Bromirski, P. D., Duennebier, F. K., and Stephen, R. A. Mid-ocean microseisms. *Geochemistry, Geophysics, Geosystems*, 6, 2005. doi: 10.1029/2004GC000768.

Burtin, A., Bollinger, L., Vergne, J., Cattin, R., and Nabelek, J. L. Spectral analysis of seismic noise induced by rivers: A new tool to monitor spatiotemporal changes in stream hydrodynamics. *Journal of Geophysical Research*, 113(B05301), 2008. doi: 10.1029/2007JB005034.

Chien, J. and Liu, Y. Effectively Distinguishing Blast and Earthquake Sources in Eastern Canada. *Seismica*, 5(1), 2026. doi: 10.26443/seismica.v5i1.1964.

Corela, C., Loureiro, A., Duarte, J. L., Matias, L., Rebelo, T., and Bartolomeu, T. The effect of deep ocean currents on ocean-bottom seismometers records. *Natural Hazards and Earth System Sciences*, 23(4):1433–1451, 2023. doi: 10.5194/nhess-23-1433-2023.

Crawford, W. and Webb, S. Identifying and removing tilt noise from low-frequency (0.1 Hz) seafloor vertical seismic data. *Bull. seism. Soc. Am.*, 90:952–963, 2000. doi: 10.1785/0119990121.

Embriaco, D. G. M., Frugoni, F., Monna, S., Etiope, G. E., Gasperini, L., Polonia, A., Del Bianco, F., Çağatay, M. N., Ulgen, U. B., and Favali, P. Monitoring of gas and seismic energy release by multiparametric benthic observatory along the North Anatolian Fault in the Sea of Marmara (NW Turkey). *Geophysical Journal International*, 196, 2014. doi: 10.1093/gji/ggt436.

Essing, D., Schlindwein, V., Schmidt-Aursch, M. C., Hadziioannou, C., and Stähler, S. C. Characteristics of current-induced harmonic tremor signals in ocean-bottom seismometer records. *Seismological Research Letters*, 92(5):3100–3112, 2021. doi: 10.1785/0220200397.

Fan, W., McGuire, J. J., and Shearer, P. M. Abundant Spontaneous and Dynamically Triggered Submarine Landslides in the Gulf of Mexico. *Geophysical Research Letters*, 47, 2020. doi: 10.1029/2020GL087213.

Galbraith, P. S., Chassé, J., Shaw, J.-L., Dumas, J., and Bourassa, M.-N. Physical Oceanographic conditions in the Gulf of St. Lawrence during 2023. *Fisheries and Oceans Canada*, 378, 2024.

Goblot, E., Liu, Y., Plourde, A., Cauchy, P., Mérindol, J., Bernier-Breton, C., Li, G., and Roth, B. Spatiotemporal variability of fin whale and blue whale calls detected by land seismometers along the Lower St. Lawrence Seaway. *Seismica*, 3(2), 2024. doi: 10.26443/seismica.v3i2.1153.

Gong, J. and Fan, W. Seismicity, fault architecture, and slip mode of the westernmost Gofar transform fault, East Pacific Rise. *Journal of Geophysical Research: Solid Earth*, 127:e2022JB024918, 2022. doi: 10.1029/2022JB024918.

Govi, M., Maraga, F., and Moia, F. Seismic detectors for continuous bed-load monitoring in a gravel stream. *Hydrological Sciences Journal*, 38(2):123–132, 1993. doi: 10.1080/02626669309492650.

Hasselmann, K. A statistical analysis of the generation of microseisms. *Reviews of Geophysics*, 1(2):177–210, 1963. doi: 10.1029/RG001i002p00177.

Hilmo, R. and Wilcock, W. S. D. Physical sources of high-frequency seismic noise on Cascadia Initiative ocean bottom seismometers. *Geochemistry, Geophysics, Geosystems*, 21, 2020. doi: 10.1029/2020GC009085.

Janiszewski, H. A., Gaherty, J. B., Abers, G. A., Gao, H., and Eilon, Z. C. Amphibious surface-wave phase-velocity measurements of the Cascadia subduction zone. *Geophysical Journal International*, 217:1929–1948, 2019. doi: 10.1093/gji/ggz051.

Klein, F. W. User's guide to HYPOINVERSE-2000, a Fortran program to solve for earthquake locations and magnitudes. *USGS Open Report*, 2002-171:123 p., 2002. doi: 10.3133/ofr02171.

Kowarski, K., Moors-Murphy, H., Maxner, E., and Cerchio, S. Western North Atlantic humpback whale fall and spring acoustic repertoire: Insight into onset and cessation of singing behavior. *The Journal of the Acoustical Society of America*, 145(4): 2305–2316, 2019. doi: 10.1121/1.5095404.

Kuna, V. M. and Nábělek, J. L. Seismic crustal imaging using fin whale songs. *Science*, 371:731–735, 2021. doi: 10.1126/science.abf396.

Kuna, V. M., Nábělek, J. L., and Braunmiller, J. Mode of slip and crust–mantle interaction at oceanic transform faults. *Nature Geoscience*, 12(2):138–142, 2019. doi: 10.1038/s41561-018-0287-1.

Lamontagne, M., Keating, P., and Perreault, S. Seismotectonic characteristics of the Lower St. Lawrence Seismic Zone, Quebec: insights from geology, magnetics, gravity, and seismics. *Can. J. Earth Sci.*, 40:317–336, 2003. doi: 10.1139/e02-104.

Liu, Y. and Harrington, R. M. Seismicity monitoring along the St. Lawrence paleorift system in Quebec [Data set]. *International Federation of Digital Seismograph Networks*, 2015. doi: 10.7914/gm3m-q077.

Liu, Y., Plourde, A., Nedimovic, M., Zhang, M., and Darbyshire, F. D. Nodal array monitoring of earthquakes and whale calls along the Lower St. Lawrence Seaway [Data set]. *International Federation of Digital Seismograph Networks*, 2023a. doi: 10.7914/tktn-xb44.

Liu, Y., Plourde, A., Nedimovic, M., Zhang, M., Darbyshire, F. D., Cauchy, P., Pellerin, A., Cairns, G., Bosman, K., and Thibodeau, J. Lower St Lawrence Ocean Bottom Experiment [Dataset]. *National Facility for Seismological Investigations*, 2023b. doi: 10.7914/x5w5-z042.

Longuet-Higgens, M. S. A theory of the origin of microseisms. *Phil. Trans. R. Soc.*, 243(857):1–35, 1950. doi: 10.1098/rsta.1950.0012.

McGuire, J. J., Collins, J. A., Lizarralde, D., Behn, M. D., Gouédard, P., van der Hilst, R. D., Roland, E., and Boettcher, M. S. Variations in earthquake rupture properties along the Gofar transform fault, East Pacific Rise. *Nature Geoscience*, 5:336–341, 2012. doi: 10.1038/ngeo1454.

McKenna, M. F., Wiggins, S. M., and Hildebrand, J. A. Relationship between container ship underwater noise levels and ship design, operational and oceanographic conditions. *Scientific Reports*, 3(1):1760, 2013. doi: 10.1038/srep01760.

McNamara, D. E. and Buland, R. P. Ambient noise levels in the continental United States. *Bulletin of the Seismological Society of America*, 94(4):1517–1527, 08 2004. doi: 10.1785/012003001.

Mellinger, D. K. and Clark, C. W. Blue whale (Balaenoptera musculus) sounds from the North Atlantic. *The Journal of the Acoustical Society of America*, 114(2):1108–1119, 2003. doi: 10.1121/1.1593066.

Mousavi, S. M., Sheng, Y., Zhu, W., and Beroza, G. C. STanford EArthquake Dataset (STEAD): A global data set of seismic signals

for AI. *IEEE Access*, 7:179464–179476, 2019. doi: 10.1109/ACCESS.2019.2947848.

Mousavi, S. M., Ellsworth, W. L., Zhu, W., Chuang, L. Y., and Beroza, G. C. Earthquake transformer—an attentive deep-learning model for simultaneous earthquake detection and phase picking. *Nature communications*, 11(1):3952, 2020.

Mérindol, M., St-Onge, G., Sultan, N., Lajeunesse, P., and Garziglia, S. Earthquake-triggered submarine landslides in the St. Lawrence Estuary (Québec, Canada) during the last two millennia and the record of the major 1663 CE M ≥7 event. *Quaternary Science Reviews*, 291:107640, 2022. doi: 10.1016/j.quascirev.2022.107640.

Münchmeyer, J. PyOcto: A high-throughput seismic phase associator. *Seismica*, 3(1), 2024. doi: 10.26443/seismica.v3i1.1130.

Niksejel, A. and Zhang, M. OBSTransformer: a deep-learning seismic phase picker for OBS data using automated labelling and transfer learning. *Geophysical Journal International*, 237(1): 485–505, 2024. doi: 10.1093/gji/ggae049.

Normandeau, A., Bourgault, D., Neumeier, U., Lajeunesse, P., St-Onge, G., Gostiaux, L., and Chavanne, C. Storm-induced turbidity currents on a sediment-starved shelf: Insight from direct monitoring and repeat seabed mapping of upslope migrating bedforms. *Sedimentology*, 67:1045–1068, 2020. doi: 10.1111/sed.12673.

NRCan. Natural Resources Canada. Canadian National Earthquake Database [Dataset]. Canadian Hazards Information Service, 1985. doi: 10.17616/R3TD24.

Nuttli, O. W. Seismic wave attenuation and magnitude relations for eastern North America. *Journal of Geophysical Research*, 78 (5):876–885, 1973. doi: 10.1029/JB078i005p00876.

Parisi, L., Augustin, N., Trippanera, D., Kirk, H., Dannowski, A., Matrau, R., Fittipaldi, M., Nobile, A., Zielke, O., Valero Cano, E., Hoogewerf, G., Aspiotis, T., Manzo-Vega, S., Espindola Carmona, A., Barreto, A., Juchem, M., Suhendi, C., Schmidt-Aursch, M., Mai, P. M., and Jónsson, S. The First Network of Ocean Bottom Seismometers in the Red Sea to Investigate the Zabargad Fracture Zone. *Seismica*, 3(1), Apr. 2024. doi: 10.26443/seismica.v3i1.729.

Plourde, A. P. and Nedimović, M. R. Earthquake depths, focal mechanisms, and stress in the Lower St. Lawrence Seismic Zone. *Seismological Research Letters*, 92(4):2562–2572, 05 2021. doi: 10.1785/0220200429.

Plourde, A. P. and Nedimović, M. R. Monitoring fin and blue whales in the Lower St. Lawrence Seaway with onshore seismometers. *Remote Sensing in Ecology and Conservation*, 8(4):551–563, 2022. doi: 10.1002/rse2.261.

Roy, N., Simard, Y., Aulanier, F., and Giard, S. Fin whale continuous frequentation of St. Lawrence habitats detected from multi-year passive acoustic monitoring (PAM). *Canadian Science Advisory Secretariat (CSAS)*, 2018(059), 2018.

Savage, B., Toomey, D., et al. Seismicity and fault structure of the Blanco Transform Fault from OBS deployments. *Geochemistry, Geophysics, Geosystems*, 18:1188–1204, 2017. doi: 10.1002/2016GC006572.

Schlindwein, V., Li, S., Kirk, H., and Schmidt-Aursch, M. C. Seismic soundscape of the Arctic Ocean: seasonal effects of sea ice and swell on deep-sea ocean bottom seismometer records. *Geophysical Journal International*, 242(1):ggaf143, 04 2025. doi: 10.1093/gji/ggaf143.

Schmandt, B., Aster, R., Scherler, D., Tsai, V., and Karlstrom, K. Multiple fluvial processes detected by riverside seismic and infrasound monitoring of a controlled flood in the Grand Canyon. *Geophysical Research Letters*, 40(18):4858–4863, 2013. doi: 10.1002/grl.50953.

Shipton, M., Obradović, J., Mišković, N., and Diamant, R. Underwater radiated noise characteristics of small vessels - An analysis of the HearMyShip database. *Marine Pollution Bulletin*, 216: 117903, 2025. doi: 10.1016/j.marpolbul.2025.117903.

Simard, Y., Roy, N., Aulanier, F., and Giard, S. Blue whale continuous frequentations of St. Lawrence habitats from multi-year PAM series. *Canadian Science Advisory Secretariat (CSAS)*, 2016 (091), 2016a.

Simard, Y., Roy, N., Gervaise, C., and Giard, S. Analysis and modeling of 255 source levels of merchant ships from an acoustic observatory along St. Lawrence Seaway. *J Acoust Soc Am.*, 140 (3), 2016b. doi: 10.1121/1.4962557.

Simard, Y., Roy, N., Giard, S., and Aulanier, F. North Atlantic right whale shift to the Gulf of St. Lawrence in 2015, revealed by long-term passive acoustics. *Endangered Species Research*, 40: 271–284, 2019. doi: 10.3354/esr01005.

St-Onge, G., Duchesne, M. J., and Lajeunesse, P. Marine geology of the St. Lawrence Estuary. *IOP Conference Series: Earth and Environmental Science*, 14, 2011. doi: 10.1088/1755-1315/14/1/012003.

St-Onge, G., Chapron, E., Mulsow, S., Salas, M., Viel, M., Debret, M., Foucher, A., Mulder, T., Winiarski, T., Desmet, M., Costa, P. J., Ghaleb, B., Jaouen, A., and Locat, J. Comparison of earthquake-triggered turbidites from the Saguenay (Eastern Canada) and Reloncavi (Chilean margin) Fjords: Implications for paleoseismicity and sedimentology. *Sedimentary Geology*, 243-244: 89–107, 2012. doi: 10.1016/j.sedgeo.2011.11.003.

Wilcock, W. S. D. Tracking fin whales in the northeast Pacific Ocean with a seafloor seismic network. *The Journal of the Acoustical Society of America*, 132(4):2408–2419, 2012. doi: 10.1121/1.4747017.

Zhang, H., Schmidt-Aursch, M. C., Geissler, W. H., and Xing, J. Characteristics of the oceanic ambient seismic noise around Tristan da Cunha in the south Atlantic from OBS data. *Journal of Geophysical Research*, 128, 2023. doi: 10.1029/2022JB025884.

Zhang, M., Ellsworth, W. L., and Beroza, G. C. Rapid Earthquake Association and Location. *Seismological Research Letters*, 90(6): 2276–2284, 09 2019. doi: 10.1785/0220190052.

Zhu, W., McBrearty, I. W., Mousavi, S. M., Ellsworth, W. L., and Beroza, G. C. Earthquake Phase Association Using Bayesian Gaussian Mixture Model. *Journal of Geophysical Research - Solid Earth*, 127(5), 2022. doi: 10.1029/2021JB023249.